# Recognition determinants of improved HIV-1 neutralization by a heavy chain matured pediatric antibody

Sanjeev Kumar[1,2,5], Swarandeep Singh[1,5], Arnab Chatterjee[3,5], Prashant Bajpai[2], Shaifali Sharma[1], Sanket Katpara[1], Rakesh Lodha[4], Somnath Dutta[3,*], Kalpana Luthra[1,6,*]

[1]Department of Biochemistry, All India Institute of Medical Sciences, New Delhi, 110029, India
[2]ICGEB-Emory Vaccine Center, International Center for Genetic Engineering and Biotechnology, New Delhi, 110067, India
[3]Molecular Biophysics Unit, Indian Institute of Science, Bangalore, 560012, India
[4]Department of Pediatrics, All India Institute of Medical Sciences, New Delhi, 110029, India
[5]These authors contributed equally
[6]Lead contact

**[*]Correspondence**

E-mail: kalpanaluthra@gmail.com, somnath@iisc.ac.in

**Keywords**

HIV-1, clade-C, N332 supersite, pediatric HIV-1 bnAb, elite-neutralizer, SOSIP trimer, cryo-EM structure

**SUMMARY**

The structural and characteristic features of HIV-1 broadly neutralizing antibodies (bnAbs) from chronically infected pediatric donors are currently unknown. Herein, we characterized a heavy chain matured HIV-1 bnAb 44m, identified from a pediatric elite-neutralizer. Interestingly, in comparison to its wild-type AIIMS-P01 bnAb, 44m exhibited moderately higher level of somatic hypermutations of 15.2%. The 44m neutralized 79% of HIV-1 heterologous viruses (n=58) tested, with a geometric mean $IC_{50}$ titer of 0.36 μg/ml. The cryo-EM structure of 44m Fab in complex with fully-cleaved glycosylated native-like BG505.SOSIP.664.T332N gp140 envelope trimer at 4.4Å resolution revealed that 44m targets the V3-glycan N332-supersite and GDIR motif to neutralize HIV-1 with improved potency and breadth, plausibly attributed by a matured heavy chain as compared to that of wild-type AIIMS-P01. This study further improves our understanding on pediatric HIV-1 bnAbs and structural basis of broad HIV-1 neutralization by 44m may be useful blueprint for vaccine design in future.

## INTRODUCTION

Extensive efforts are currently ongoing worldwide to develop a safe and effective human immunodeficiency virus-1 (HIV-1) vaccine. During HIV-1 infection, neutralizing antibodies (nAbs) are elicited against the envelope (env) glycoprotein gp160[1–3]. Highly potent broadly neutralizing antibodies (bnAbs) are found to develop and evolve in only top 1% of HIV-1 infected individuals, classified as elite-neutralizers[4,5]. So far, seven distinct epitopes of HIV-1 bnAbs have been identified to be present on the viral env that are: V2-apex, V3-glycan N332-supersite, CD4 binding site (CD4bs), silent-face center (SFC), membrane-proximal external region (MPER), gp120–gp41 interface and fusion peptide (FP)[3]. The prime goal is to design and develop an HIV-1 vaccine capable of triggering naïve B cells and steer them to evolve into bnAb generating B cells upon immunization/vaccination[6–8].

HIV-1 infected infants have been shown to develop bnAb responses within one year of age[9,10] while in infected adults, it takes at least 2 to 3 years post infection for the development of bnAbs[4,11,12], suggesting distinct maturation pathways of the bnAbs evolving in children[9,13]. The HIV-1 bnAbs isolated from adults have been extensively characterized, both structurally and functionally; with some of them exhibiting characteristic features of high somatic-hypermutations (SHM) and long CDR3 regions[3], while there is a paucity of such information on the bnAbs generated by HIV-1 infected children. A number of studies carried out on HIV-1 infected pediatric cohorts have reported HIV-1 plasma bnAb responses targeted at multiple env epitopes including the V2-apex, N332-glycan supersite, CD4bs and MPER[9,10,14–21]; however only two pediatric HIV-1 bnAbs have been reported thus far: BF520.1[10] and AIIMS-P01[22]. Binding of both AIIMS-P01 and BF520.1 are dependent on the N332-supersite epitope present at the base of the V3-glycan region[10,22]. Both pediatric bnAbs exhibit limited SHM (~7%); however, there is paucity of information towards understanding whether an increased SHM can be acquired in bnAbs evolving in HIV-1 infected children and further, if the increased SHM in pediatric bnAbs can lead to increase in their potency and breadth of viral neutralization, as observed in bnAbs evolving in HIV-1 infected adults[1,3,23–32].

Immunogenetic information of HIV-1 bnAbs from adults and children derived from deep sequencing or single cell analysis of B cell repertoire (BCR) can further our understanding of their natural development during the course of infection and development of blueprints for rational vaccine design and effective vaccination strategies[6,7]. Furthermore, structural characterization of

potent bnAbs, in complex with native-like trimeric env can provide useful mechanistic insights for broad and potent neutralization of HIV-1 heterologous viruses.

We previously reported the isolation of a bnAb AIIMS-P01, from an antiretroviral naïve HIV-1 clade-C chronically infected pediatric elite-neutralizer AIIMS_330[15,20,22,33,34]. Recently, for the first time, we identified several adult HIV-1 bnAbs clonotypes targeting multiple epitopes in a pair of monozygotic twin pediatric elite-neutralizers AIIMS_329 and AIIMS_330 from longitudinal (3 time points samples) bulk B cell repertoire analysis by next-generation sequencing (NGS)[35]. Herein, to delineate the characteristics of an affinity matured lineage member antibody of our previously discovered AIIMS-P01 pediatric bnAb, we performed the structural and functional characterization of a heavy chain matured pediatric HIV-1 AIIMS-P01 bnAb lineage monoclonal antibody clone 44m (referred to as 44m). The 44m exhibited moderate level of SHM (15.2%) and demonstrated near about 79% HIV-1 neutralization breadth with ~2 times improved potency than AIIMS-P01 wild-type (WT) bnAb. Cryo-EM analysis of 44m in complex with native-like fully cleaved and glycosylated BG505.SOSIP.664.T332N gp140 trimer revealed structural insights that may attribute to its neutralization breadth.

## RESULTS

### Identification of a matured AIIMS-P01 lineage antibody

We previously reported the isolation and characterization of a broad and potent anti-HIV-1 bnAb AIIMS-P01 from an Indian clade-C infected pediatric elite-neutralizer AIIMS_330[22]. Recently, for the first time, we identified several adult HIV-1 bnAbs clonotypes targeting multiple epitopes in monozygotic twins pediatric elite-neutralizers AIIMS_329 and AIIMS_330 from longitudinal (3 time points samples) bulk B cell repertoire analysis by NGS[35]. Based on our analysis pipeline we identified few (n=21) matured AIIMS-P01 bnAb heavy chain lineage members/clonotypes (**Figure 1A and S1; Table S1 and S2**) from the year 2018 time point of the AIIMS_330 pediatric elite-neutralizer, from whom AIIMS-P01 was isolated previously[20,22,35]. These 21 heavy chain sequences shared the same clonotype with AIIMS-P01 pediatric HIV-1 bnAb, with varied and moderate level (30 nt – 47 nt) of somatic hypermutations (SHM) (**Table S2**). The clonotypes were defined as sequences sharing the same V and J genes, having same CDRH3 length and more than 80% CDRH3 identity (**Table S2**). Like AIIMS-P01 WT bnAb, all 21 matured lineage members maintained the presence of 5 amino acid (AA) indel in the heavy chain framework region 3 (FRH3), however, the mature lineage members exhibit the indel 'SDPIR' instead of 'SNPSR' which is present in the AIIMS-

92 P01 WT bnAb (**Figure S1 and Table S2**)[22]. Next, we calculated the antibody mutation probabilities
93 using ARMADiLLO, an online server developed to identify both improbable and probable
94 mutations[36]. Interestingly, we found the presence of 4 improbable mutations with less than 2%
95 frequency in the 44m antibody (**Figure S2**) when we analyzed the 44m sequence using
96 ARMADiLLO method[36,37]. The CDRH3 region of the matured lineage members showed the
97 presence of varied mutations (**Figure 1B and Table S2**). We did not find matched CDRL3 light
98 chain genes as that of the AIIMS-P01 from our sequencing data. As observed by us previously, the
99 heavy chain, specifically heavy chain 5 AA indel dominantly contributed to recognition of N332-
100 supersite, HIV-1 neutralization breadth and autologous virus neutralization[22]. Therefore, to
101 evaluate the effect of higher level of SHM in matured AIIMS-P01 lineage members, herein, we
102 synthesized a matured (15.2% SHM) AIIMS-P01 bnAb heavy chain gene with >80% similar CDRH3
103 sequence as of AIIMS-P01, designated as 44m and expressed the mAb by co-transfecting plasmids
104 carrying this heavy chain gene and the WT AIIMS-P01 light chain gene. The SHM in 44m antibody
105 heavy chain gene was compared to AIIMS-P01 WT and other HIV-1 bnAbs (**Figure 1C**).

106 **Matured antibody 44m showed broader and more potent HIV-1 neutralization than AIIMS-**
107 **P01**

108 Next, we assessed the binding reactivity of the matured 44m mAb to heterologous HIV-1
109 BG505.SOSIP.664.T332N gp140 trimeric envelope protein in comparison to AIIMS-P01 WT and
110 observed high binding efficiency (**Figure 1D**). To further validate the binding data obtained by
111 ELISA, affinity analysis of the 44m with HIV-1 BG505.SOSIP.664.T332N gp140 trimer was
112 performed using Octet BLI assays. Antibody 44m showed high nanomolar (nM) affinity (KD: 0.56
113 nM) with the BG505.SOSIP.664.T332N gp140 envelope trimer (**Figure 1E**). The neutralization
114 potential of 44m antibody was tested against heterologous viruses and global panel of HIV-1
115 viruses, at concentrations ranging from 10μg/ml to 0.001 μg/ml, using a TZM-bl based
116 neutralization assay[38]. The 44m antibody neutralized 77% HIV-1 clade-C viruses and 80% clade-
117 B viruses and demonstrated an overall improvement of breadth of 79% against the heterologous
118 viruses tested, and potency, with a geometric mean $IC_{50}$ titer of 0.36 μg/ml, as compared to 67%
119 exhibited by AIIMS-P01 previously[22]. Further, a 58% breadth, with $IC_{50}$ titer of 0.43 μg/ml was
120 observed, on testing this bnAb against the global panel of viruses (**Figure 2A and 2B**). The
121 neutralizing activity data reveal an increase in potency and breadth of the matured version 44m
122 against the heterologous viruses tested (**Figure 2C**). These findings encouraged us to perform
123 structural characterization of 44m antibody with the stabilized envelope BG505.SOSIP.664.T332N
124 gp140 trimer.

125 **Cryo-EM based structural analysis of 44m in complex with BG505.SOSIP.664.T332N gp140**
126 **trimer**

127 A structural insight into mature 44m antibody in complex with BG505.SOSIP.664.T332N gp40
128 trimer was achieved through single particle cryo-Electron Microscopy (cryo-EM) and a high-
129 resolution structure was solved at 4.4 Å resolution (**Figure 3 and S3–S6**). The atomic model fitted
130 in the EM map of BG505.SOSIP.664.T332N gp140 trimer in complex with Fab of the
131 44m bnAb displayed a total of three 44m Fabs, with one Fab bound to each protomer of the Env
132 trimer for effective neutralization (**Figure 3 and S3**). Cryo-EM structures of
133 BG505.SOSIP.664.T332N gp140 Env trimer with 44m bnAb indicated trimeric shapes of HIV
134 trimer, which additionally connected with extra densities, attributed to the corresponding bound
135 Fab moieties (**Figure S4B**). Different subdomains, gp120, gp41 and Fab densities were visible in
136 the high-resolution cryo-EM structure of the Env trimer in complex with 44m bnAb (**Figure 3**).

137 Structural analysis revealed that the CDRH3 loop of neutralizing antibody 44m stretched deep
138 inside the groove between the N295 and N332 residues, thus reaching the base of the V3 loop of
139 gp120 and established a range of chemical bonds with the nearby favorable amino acids (**Figure**
140 **4A**). The total occupied surface area of 44m is ~750 $Å^2$, with extensive participation of the heavy
141 chain. This surface area includes all the CDR regions and FR3 region, but the CDRH1 and CDRH3
142 loop show a predomination contribution. The positioning of the CDR regions of the heavy chain is
143 crucial to establish contact points with the V3 loop of the gp120 (**Figure 4A, B**). The key residues
144 on the CDRH3 loop of 44m mAb that are interacting with the gp120 region are V106, P107, A108,
145 R109, and W110, whereas the primary contact points of CDRH1 and CDRH2 loops with the V3-
146 region are H31, Y52, Y53, T54, D56, and T57 (**Figure 4B**). These interactions are mainly stabilized
147 by both hydrogen bonding and van der Waals interactions. Interestingly, the R109 residue of the
148 CDRH3 demonstrated a salt bridge interaction with the D325 residue of GDIR motif of the
149 envelope gp120 region (**Figure 4C**). These interacting residues are hidden within the different
150 clefts of the V3 loop of the gp120 region. The surface potential map of the paratope region depicts
151 the interacting residues of CDR regions placed near the polar residues of the V3 loop (**Figure 4D**
152 **and S7**).

153 **Pediatric HIV-1 bnAb 44m primarily recognizes V3-glycans**

154 The antibody-Env protein interaction studies unraveled the possibilities to explore the glycan
155 antibody interactions. The atomic model demonstrated that the interaction sites for 44m bnAb on

156 gp120 were positioned in an area that is surrounded by the N-glycan patches: Asn301, Asn332
157 located near the base of V3, Asn156 glycan in the V1V2 region, and Asn295 glycan near the bottom
158 of gp120 (**Figure 5A-D**), though no interactions were observed with Asn156 and Asn295 glycans.
159 This binding approach created an interlocked system of $V_H$ loop of 44m and V3 loops of gp120,
160 and forming a stable antibody-antigen complex (**Figure 5B**). Glycan binding to N301 is forming
161 contacts with polar and charged amino acids of the CDRH2 loop, wherein the T54 and D56 of the
162 CDRH2 region are interacting with the polar side of glycan moieties to mask the binding to host
163 cells (**Figure 5C**). The N332 glycan engages in forming the largest interacting area, with most of
164 the CDRH3 region involving different portions of glycan moieties on it. N-Acetyl glucosamine
165 (NAG) attached to the N332 residue and forms a hydrogen bonding with Ser111 and Tyr113
166 residues of the CDRH3 region (**Figure 5D**). Overall, the structural analysis showed that the 44m
167 antibody interacts with different glycan moieties attached to asparagine residues at 301 and 332
168 positions in the V3 region.

169 **44m showed distinct glycan binding interactions, with similar pattern of epitope**
170 **interaction like other V3-glycan bnAbs**

171 A comparative structural analysis of the 44m antibody with other available bnAbs (BG18, 10-1074,
172 DH270.6 & BF520.1) was performed to understand the exceptionality of this 44m antibody
173 (**Figure S7 – S9**). Superimposition of the antibodies directed at the V3 loop region of the gp120
174 protomer showed a common interaction pattern across all the bnAbs within the V3 region. In the
175 BG18 bnAb (6dfg) CDRL3 and CDRH3 loops are interacting with V3 region for stalking of the
176 antibody onto the gp120 (**Figure S9A**). In bnAb 10-1074 (6udj), the V3 loop of gp120 protomer
177 interacts with CDRH3 and CDRL3 regions (**Figure S9B**). DH270.6 (6um6) and BF520.1 (6mn7)
178 have more inter-facial area**,** which helps in the interaction of residues in CDRL1 and CDRL2
179 regions. Additionally, the V1 region interacts with the CDRL3 loop (**Figure S9C, D**). The V3 loop
180 has stable bonding with the CDRH1 loop for effective neutralization. The presence of an 8 amino
181 acid long elongated face in the CDRH3 region in PGT121 and PGT122 classes of antibodies make
182 these antibodies potent to bind gp120 surface using two functional surfaces (**Figure S9E**). These
183 results suggest that the overall binding region of the CDR with both V3 and V1/V2 loops were
184 significantly increased. The superimposition of V3-glycan bnAbs into the gp120 trimer depicts the
185 variability in the binding surface area but a common binding pattern on the gp120.

186 **44m HIV-1 bnAb showed co-dependence on GDIR motif and N332-supersite**

187 Results obtained from structural mapping of 44m showed that this bnAb binds the N301, D325
188 residue of GDIR motif and N332-supersite env regions (**Figure 4 and 5**). Next, we used this
189 structural mapping information to understand the linkage of these residues in 44m mediated HIV-
190 1 neutralization by performing sequence alignment of these identified contact residues within the
191 envelope regions of the viruses tested (**Figure S10**). The analysis revealed that the N156 and N301
192 glycans are relatively conserved among the 44m susceptible viruses (**Figure S10**). In contrast,
193 mutations present at D325 and N332 positions were found to be associated with abrogation in
194 neutralization potential of 44m and vice-versa, e.g. HXB2, ZM249 and ZM233 viruses were
195 resistant to neutralization by 44m, due to the absence of GDIR epitope in these viruses. To further
196 confirm the reliance of the 44m mAb on the D325 residue, we conducted functional mutant assays
197 and noted a 59-fold decrease in the presence of the D325K mutation, highlighting the dependence
198 on the GDIR motif (**Figure S11**). These findings suggest that the neutralization dependence of the
199 pediatric bnAb 44m relies on the D325 residue of GDIR motif and N332-spersite, as has also been
200 reported for the adult HIV-1 V3-glycan directed bnAbs PGT121 and 10-1074[26,39].

201 **DISCUSSION**

202 The footprints of HIV-1 broadly neutralizing antibodies (bnAbs) can provide a template for
203 structure-guided vaccine design[6,7]. Highly potent bnAb based therapeutics, prophylactics and
204 vaccines are attractive strategies to tackle HIV-1[3]. Immunogenetics based information of potent
205 HIV-1 bnAbs derived from deep sequencing or single cell analysis of B cell repertoire (BCR) of
206 infected donors can provide critical insights towards understanding their natural development
207 during the course of infection and reveal the frequency of B cells within the human B cell
208 repertoire, that can elicit potent bnAbs to guide vaccination strategies[6,29,40,41]. Further, the
209 structural characterization of potent HIV-1 bnAbs in complex with the viral envelope provides
210 useful mechanistic insights of viral neutralization and information of epitope-paratope interaction
211 for rational vaccine design[7]. Currently, the leading strategy in innovative HIV-1 next-generation
212 immunotherapeutic and vaccine design is to develop and elicit bnAb responses by steering bnAb
213 expressing B cells[6,8]. To achieve this goal, it is essential to understand the structural mechanism of
214 HIV-1 neutralization and immunogenetics of B cells that elicit potent bnAbs. The evolution of HIV-
215 1 bnAbs from adult donors has been studied extensively[29,42,43], but, no information is available on
216 the evolving HIV-1 bnAb lineage in chronically infected children.

217 Herein, to fill this knowledge gap, we synthesized a heavy chain matured lineage member (44m)
218 of AIIMS-P01 bnAb identified from our recent study on identification of multiple epitopes

219 targeting adult HIV-1 bnAbs clonotypes in AIIMS_330 pediatric elite-neutralizer from longitudinal
220 bulk B cell repertoire analysis by NGS[35]. We further evaluated the structural features and
221 functionality of 44m antibody in terms of viral binding and neutralization activity. We used only
222 heavy chain of AIIMS-P01 matured lineages as we didn't find matched CDRL3 of the AIIMS-P01
223 light chain in our deep sequencing data, plausibly due to the low depth of sequencing[35]. We
224 combined functional and structural approaches and showed that maturation in the 44m heavy
225 chain, like that reported for the adult bnAbs of the PGT class[42,44], was functionally important for
226 HIV-1 Env binding and neutralization. This was demonstrated by the increased heterologous
227 breadth observed when the mature heavy chain was paired with the original light chain of AIIMS-
228 P01 WT bnAb, suggesting that the recently acquired SHMs can be functionally important for the
229 evolution and neutralization breadth for this bnAb. In addition, the matured bnAb 44m exhibited
230 a change of indel sequence (SNPSR mutated to SDPIR), in comparison to its WT bnAb AIIMS-P01
231 (**Figure S1**).

232 Unlike HIV-1 CD4bs bnAbs, the V3-glycan targeting bnAbs are of high interest because they are
233 common and not restricted by certain germline genes[1,3]. The pediatric bnAb AIIMS-P01 and infant
234 derived BF520.1 are of particular interest because these showed broad HIV-1 neutralization
235 despite limited SHM[10,22]. The 44m lineage bnAb identified and characterized herein showed
236 improved neutralization potency and breadth plausibly by acquisition of higher number of SHM,
237 that led to an increase in potency twice that of the WT AIIMS-P01 bnAb. To estimate the
238 probability of amino acid SHM substitutions in the 44m heavy chain we used the ARMADiLLO
239 method as described previously . Interestingly, we identified 4 improbable AA SHM in 44m bnAb
240 with less than 2% frequency. The probability of antibody mutations can be useful to vaccinologists
241 in designing vaccines to elicit such bnAbs which are enriched with developmentally rate-limiting
242 improbable mutations[36,37].

243 The cryo-EM structural analysis of bnAb 44m, indicated that CDRH1 (H31, Y53 and T57) and
244 CDRH3 (P107, A108 and R109) residues appear to contribute to the 44m paratope by mediating
245 contacts with the conserved V3-glycan N332-supersite, D325 of 'GDIR' sequence motif, glycans at
246 position 301 and 332. These major determinants of neutralization breadth interacting with
247 residues within the CDRH1 and CDRH3 regions of the 44m, are similar to that in the adult bnAbs
248 and distinct from the infant bnAb BF520.1[10,42]. The angle of approach by 44m towards the V3
249 epitope was previously determined to be similar to PGT121[39,45], although the positioning of 44m
250 was notably different and slightly rotated relative to the PGT121. The crystal structure of PGT121
251 in complex with gp120 identified the GDIR motif and glycans at positions N332 and N301 as the

252 primary contacts defining the PGT121 epitope[39,45]. The CDRH3 loop, which is highly mutated in
253 PGT121, penetrates the glycan shield in order to contact both the GDIR motif and N332 glycan.

254 The structural model similarly indicates potential CDRH3 contacts with the GDIR motif and N332
255 glycan. However, structurally defined epitope-paratope interface do not fully capture the
256 functional binding contacts that drive neutralization and escape[46], reinforcing the gravity of
257 functional assays to define the recognition determinants that are important for neutralization
258 activity. As we demonstrated previously the WT mAb AIIMS-P01 does not show the dependence
259 on V1 glycan N156[22], likewise the structural analysis of mutant 44m suggests N156 is hanging out
260 of the core, without making dominant interactions. Though we observed that 44m epitope is
261 surrounded with other V3-region glycans including N295 and N301, however, HIV-1 viral
262 sequence alignment (**Figure S10**) revealed that 44m is primarily dependent on N332-glycan
263 supersite and GDIR motifs. To further validate the 44m mAb dependence on D325 residue, we
264 performed functional mutant assays and observed a 59-fold decrease in case of D325K mutation
265 indicating dependence on GDIR motif (**Figure S11**). Based on the findings of HIV-1 binding,
266 neutralization and structural analysis of the 44m pediatric bnAb, we postulate that a germline
267 targeting vaccine / immunogen could potentially elicit AIIMS-P01 / 44m-like responses. In the
268 AIIMS_330 pediatric elite neutralizer, the circulating and coevolving viruses may have led to
269 elicitation of this bnAb lineage (44m), to drive affinity maturation in the AIIMS-P01 bnAb, as has
270 been observed previously for the evolution of V1V2 and V3-glycan plasma bnAbs[20].

271 In summary, the structural and functional characterization of a heavy chain matured pediatric
272 bnAb 44m showed improved HIV-1 neutralization potency and breadth in comparison to its WT
273 bnAb AIIMS-P01. This study for the first time provides evidence towards contribution of antibody
274 SHM in improved HIV-1 neutralizing efficiency of a bnAb identified from a pediatric donor living
275 with chronic HIV-1 clade C infection. Further studies in this direction are required to be conducted
276 to understand the antigenic triggers in chronically infected children that can elicit similar
277 protective bnAbs targeting other HIV-1 bnAb epitopes which in turn can provide a blueprint to
278 guide HIV-1 vaccine design.

279 **Limitations of the study**

280 Our work is focused on the binding, neutralization, and structural characterization of a matured
281 lineage member (44m) of AIIMS-P01 pediatric HIV-1 bnAb. All conclusions are based on cryo-EM
282 structural analysis, genetic features analysis and in-vitro HIV-1 viral neutralization assays. The

283 bulk B cell repertoire of total PBMCs led to identification of only few AIIMS-P01 heavy chain
284 lineage members/clonotypes and no light chain sequences were identified. An in-depth NGS based
285 sequencing of AIIMS-P01 lineage will enable the identification of a large number of clonotypes for
286 in depth characterization of bnAb lineages.

287 **MAIN FIGURE TITLES AND LEGENDS**

288 **Figure 1: Characterization of AIIMS-P01 lineage members/clonotypes.**
289 **(A)** Phylogenetic tree of AIIMS-P01 lineage based on heavy chain sequences.
290 **(B)** Logogram representing the frequency of the amino acid residues in CDRH3 of lineage mAbs.
291 **(C)** Somatic hypermutation (SHM) analysis of HIV-1 adult and pediatric bnAbs shown as %
292 nucleotide (Nt) mutations relative to respective germline variable gene sequence. Here, pediatric
293 HIV-1 bnAbs are highlighted in red color.
294 **(D)** Binding reactivity of the 44m and AIIMS-P01 mAbs to HIV-1 BG505.SOSIP.664.T332N gp140
295 trimeric envelope protein determined by ELISA.
296 **(E)** Binding Affinity of 44m to BG505.SOSIP.664.T332N gp140 envelope trimer determined by
297 Octet BLI.
298 See also **Figure S1, S2 and Table S1 and S2**.

299 **Figure 2: Matured AIIMS-P01 lineage antibody 44m showed broad HIV-1 neutralization**
300 **with improved potency.**
301 **(A)** Heat map depicting $IC_{50}$ values of the 44m tested against heterologous panel of HIV-1 viruses,
302 using a TZM-bl based neutralization assay (n=58).
303 **(B)** Heat map depicting $IC_{50}$ values of the matured 44m mAb tested against HIV-1 global panel.
304 **(C)** Neutralization breadth comparison of HIV-1 adult and pediatric bnAbs is shown. Here,
305 pediatric HIV-1 bnAbs are highlighted in red color. The graph was plotted using Prism software.
306 The neutralization potency ($IC_{50}$) of 44m bnAb is compared with the $IC_{50}$ of other HIV-1 bnAbs as
307 documented in the Los Alamos HIV-1 molecular immunology database.

308 **Figure 3: Cryo-EM reconstruction and model of BG505.SOSIP.664.T332N gp140 trimer in**
309 **complex with 44m bnAb.**
310 **(A)** Side and top views of cryo-EM reconstructed map of BG505.SOSIP.664.T332N gp140 trimer
311 in complex with 44m bnAb solved at ~4.4Å resolution, with a local resolution in between 3.36 and
312 3.74Å. Color coding corresponding to segmented EM densities are: orange red, 44m bnAb; lime
313 green, gp120; pink, gp41.

314 **(B)** The corresponding atomic model fitted in the EM map of BG505.SOSIP.664.T332N gp140
315 trimer in complex with 44m bnAb showing three 44m bnAb binds to each gp120 monomeric
316 subunit for effective neutralization.
317 See also **Figure S3 – S6 and Table S3**.

318 **Figure 4: Interaction sites for 44m bnAb to form a complex with BG505.SOSIP.664.T332N**
319 **gp140 trimer.**
320 **(A)** The CDR regions in the interface of gp120 and 44m bnAb are highlighted using color coding:
321 magenta, FR3; green, CDRH1, olive green, CDRH2; and, cyan, CDRH3; dodger blue, CDRL1; deep
322 sky blue, CDRL2; median blue, CDRL3.
323 **(B)** Salt bridge interaction in between D325 residue in the V3 loop of envelope gp120 monomer
324 and CDRH1 region, where D325 is shown in dark green and R109 is shown in purple color, and
325 the bond is shown in red color.
326 **(C)** Different interacting partners in the epitope region to adapt a stable conformational state with
327 the CDR regions.
328 **(D)** Electrostatic potential surface map of the interacting region of gp120 showing the interacting
329 residues of the paratope facing towards the charged residues of the epitope. The residues on 44m
330 bnAb is shown in golden color.
331 See also **Figure S7 – S11**.

332 **Figure 5: Glycan interaction sites of BG505.SOSIP.664.T332N gp140 trimer in complex with**
333 **44m Fab.**
334 **(A)** Positions and fitting different glycan residues are pointed in the EM map shown. In the atomic
335 model N301 and N332 glycans are shown in orange color, whereas the Fab and CDR regions are
336 colored similarly to Figure 2.
337 **(B)** The gp120 monomer is shown in gray. Atomic model illustrating various glycan residues
338 interacting with different region of CDR regions of 44m bnAb, where glycan attached to N156 is
339 coming closer to CDRH1 region.
340 **(C)** The NAG attached to Asn301 is making contact points with Thr54 and Asp56 in the CDRH2
341 region (shown in olive drab color).
342 **(D)** Glycan binding to Asn332 is interacting with Ser111 and Tyr113 residues of the CDRH3 region
343 (shown in deep blue color).
344 See also **Figure S8 – S11**.

## STAR ★ METHODS

Detailed methods are provided in the online version of this paper and include the following:

- **KEY RESOURCES TABLE**
- **RESOURCE AVAILABILITY**
  - Lead contact
  - Materials availability
  - Data and code availability
- **EXPERIMENTAL MODEL AND STUDY PARTICIPANT DETAILS**
  - Cell Lines
- **METHOD DETAILS**
  - Identification of AIIMS-P01 lineage members
  - 44m heavy chain SHM analysis using ARMADiLLO method
  - Antibody gene synthesis
  - Antibody genes sequence analysis
  - Expression of monoclonal antibodies
  - Expression and purification of HIV-1 trimeric proteins
  - Binding analysis of mAbs by ELISA
  - HIV-1 pseudovirus generation
  - HIV-1 neutralization assays
  - Fab Fragment Preparation
  - Octet BLI analysis
  - Negative-stain EM
  - Sample preparation for cryoEM
  - CryoEM data acquisition
  - CryoEM data analysis and model building
- **QUANTIFICATION AND STATISTICAL ANALYSIS**

## KEY RESOURCES TABLE

| REAGENT or RESOURCE | SOURCE | IDENTIFIER |
|---|---|---|
| **Antibodies** | | |
| Goat Anti-Human IgG (Fc), alkaline phosphatase (AP) | Southern Biotech | Cat #2048-04; RRID: AB_2795687 |
| AIIMS-P01 | Kumar et.al., 2019[22] | PMID: 30429339 |
| 44m | This Study | N/A |
| | | |

| **Bacterial and virus strains** | | |
|---|---|---|
| Panel of Global HIV-1 Env Clones | NIH AIDS Reagent Program | Cat#12670 |
| Panel of HIV-1 Subtype C Env Clones | NIH AIDS Reagent Program | Cat#11326 |
| Panel of HIV-1 Subtype B Env Clones | NIH AIDS Reagent Program | Cat#11227 |
| HIV-1 Env Molecular Clones - Panel of Subtype C Indian Env clones | NIH AIDS Reagent Program | Cat#11672 |
| PSG3ΔEnv | NIH AIDS Reagent Program | Cat#11051 |
| AIIMS_706_70606F | Mishra et.al. Nat. Comm. 2020[17] | Accession: MN703355 |
| AIIMS_706_70606Z | Mishra et.al. Nat. Comm. 2020[17] | Accession: MN703353 |
| AIIMS_706_70607B | Mishra et.al. Nat. Comm. 2020[17] | Accession: MN703356 |
| AIIMS_706_70606B | Mishra et.al. Nat. Comm. 2020[17] | Accession: MN703359 |
| AIIMS_706_70604B | Mishra et.al. Nat. Comm. 2020[17] | Accession: MN703352 |
| AIIMS_706_70607C | Mishra et.al. Nat. Comm. 2020[17] | Accession: MN703357 |
| AIIMS_704_70406 | Mishra et.al. Nat. Comm. 2020[17] | Accession: MN703348 |
| AIIMS_704_70408 | Mishra et.al. Nat. Comm. 2020[17] | Accession: MN703349 |
| AIIMS_704_70402 | Mishra et.al. Nat. Comm. 2020[17] | Accession: MN703345 |
| AIIMS_709_709316B | Mishra et.al. Nat. Comm. 2020[17] | Accession: MN703365 |
| AIIMS_330_330_16_E6 | Mishra et.al. JVI. 2019[20] | Accession: MK076720 |
| AIIMS_329_329_16_B1 | Mishra et.al. JVI. 2019[20] | Accession: MK076641 |
| DH5α, *E.Coli* | Thermo Scientific, USA | Cat#18265017 |
| | | |
| **Chemicals, peptides, and recombinant proteins** | | |
| Tween 20 | Fisher Scientific | Cat#BP337-500 |
| Pierce™ Protein A Agarose resin | Thermo Fisher Scientific | Cat# 20334 |
| ExpiFectamineTM 293 trans-fection reagent | Thermo Fisher Scientific | Cat# A14524 |
| Expi293™ Expression Medium | Thermo Fisher Scientific | Cat# A1435102 |
| DEAE-Dextran | Sigma, USA | Cat#D9885-10G |
| DMEM | Hyclone, GE Healthcare, USA | Cat#SH30243.01 |
| RPMi-1640 | Hyclone, GE Healthcare, USA | Cat#SH30027.01 |
| Fetal Bovine Serum, US Origin | Hyclone, GE Healthcare, USA | Cat#SH30071.03 |
| QIAGEN Plasmid Plus Midi Kit (100) | QIAGEN, Germany | Cat#12145 |
| QIAGEN Plasmid Plus Maxi Kit (100) | QIAGEN, Germany | Cat#12362 |
| QIAprep Spin Miniprep Kit (250) | QIAGEN, Germany | Cat#12123 |
| QIAquick PCR & Gel Cleanup Kit (100) | QIAGEN, Germany | Cat#28706 |
| DNA Sequencing | NA | Eurofins, India |
| | | |
| **Critical commercial assays** | | |

| | | |
|---|---|---|
| Bright-Glo Luciferase Assay System | Promega | Cat#E2610 |
| Quick-change II XL Site-Directed Mutagenesis Kit | Agilent Technologies | Cat#200522 |
| | | |
| **Deposited data** | | |
| mAb sequences | This study | Supplementary Material |
| EM Map of BG505.SOSIP.664.T332N gp140 trimer complexed with mAb 44m | This study | EMD: 36815 |
| | | |
| **Experimental models: Cell lines** | | |
| Expi293F cells | Thermo Scientific, USA | Cat# A14527; RRID: CVCL_D615 |
| HEK293T | ATCC | Cat#CRL-3216; RRID: CVCL_0045 |
| TZM-bl | NIH AIDS Reagent Program | Cat#8129; RRID: CVCL_B478 |
| | | |
| **Recombinant DNA** | | |
| AbVec antibody expression vectors | Kumar et.al., 2019[22] | PMID: 30429339 |
| | | |
| **Software and algorithms** | | |
| GraphPad Prism (v9) | GraphPad Software, Inc. | GraphPad Prism https://www.graphpad.com:443/; RRID: SCR_002798 |
| Coot | Emsley et al., 2010 [47] | https://www2.mrc-lmb.cam.ac.uk/personal/pemsley/coot/; RRID: SCR_014222 |
| PHENIX | Adams et al., 2010 [48] | https://phenix-online.org; RRID: SCR_014224 |
| UCSF ChimeraX | Goddard et al., 2018 [49] | https://www.cgl.ucsf.edu/chimerax/; RRID: SCR_015872 |
| Molprobity | Williams et al., 2018 [50] | http://molprobity.biochem.duke.edu/; RRID: SCR_014226 |
| IMGT/HighV-QUEST | Lefranc et.al., 2009 [51] | http://imgt.org/HighV-QUEST; RRID: SCR_010749 |
| Relion 3.1 | Scheres, 2012 [52] | https://www3.mrc-lmb.cam.ac.uk/relion/index.php/Main_Page; RRID: SCR_016274 |
| **Other** | | |
| Octet Red96 | Fortebio | N/A |

372

373 **RESOURCE AVAILABILITY**

374 **Lead contact**

375 Further inquiries and requests for data, plasmids and resources should be directed to the lead
376 contact Kalpana Luthra (kalpanaluthra@gmail.com).

377 **Materials availability**

378 Antibody expression plasmids generated in this study (see key resources table) are available upon
379 request from the lead contact with a completed Materials Transfer Agreement.

380 **Data and code availability**

381 • Atomic coordinates and cryo-EM maps for reported structures are deposited into the Elec-
382 tron Microscopy Data Bank (EMDB) with accession code EMD-36815 for BG505.SO-
383 SIP.664.T332N gp140 envelope trimer in complex with mAb 44m. The sequences of the
384 44m and AIIMS-P01 lineage antibody heavy chain variable regions are present in the sup-
385 plementary materials. Raw sequence data that support the findings in this study has been
386 deposited at NCBI Sequencing Read Archive (www.ncbi.nlm.nih.gov/sra) and publicly
387 available under BioProject accession number SRA: PRJNA999025. Processed datasets are
388 available at https://github.com/prashantbajpai/HIV_BCR_Analysis.

389 • All code for analysis and generating individual figure panels are available on GitHub and
390 link to the repository is https://github.com/prashantbajpai/HIV_BCR_Analysis.

391 • Any additional information required to reanalyze the data reported in this paper is availa-
392 ble from the lead contact upon request.

393 **EXPERIMENTAL MODEL AND STUDY PARTICIPANT DETAILS**

394 **Cell Lines**

395 Human embryonic kidney (HEK)-derived 293T, and HeLa-derived TZM-bl cells were main-
396 tained in complete Dulbecco's Modified Eagle Medium (herein referred to as cDMEM) contain-
397 ing high glucose Dulbecco's Modified Eagle Medium (DMEM, Thermo Fisher), 1X Penicillin-
398 Streptomycin (Pen Strep, Thermo Fisher) and 10% fetal bovine serum (FBS, Gibco) at $37^0$C
399 and 5% $CO_2$. FreeStyle 293F and Expi293F cells (Thermo Fisher) were maintained in Freestyle

400 293 Expression Medium and Expi293 Expression Medium, respectively, at 37$^0$C and 8 % CO2
401 with shaking at 120 RPM.

402 **METHOD DETAILS**

403 **Identification of AIIMS-P01 lineage members**

404 We recently reported the deep sequencing of bulk B cell repertoire (BCR) that was performed
405 using primers, protocols and Illumina MiSeq (MiSeq Reagent Kit v3, 600-cycle) as described
406 previously[35,53]. The Abstar analysis pipeline was used as previously described to quality trim,
407 remove adapters and merge paired sequences[53]. Sequences were then annotated with Abstar in
408 combination with UMI based error correction by AbCorrect
409 (https://github.com/briney/abtools/). For comparison of frequencies, read counts were scaled
410 for each repertoire as previously described due to the large differences in the number of reads
411 between each group. Somatic hypermutation (SHM) was calculated using the R package Shazam[54].
412 Clonotype analysis was performed using Immcantation pipeline[54,55]. Sequences were grouped into
413 clonotypes based on nucleotide hamming distance of 0.16 calculated based on bimodal
414 distribution of distance of each sequence with its nearest neighbor. Alternatively, sequences were
415 also clustered into clonal groups using an in-house script. The criteria used for clonal assignment
416 was sequences having same V and J gene usage, same CDRH3 length and at least 80% CDRH3
417 amino acid identity. Germline V(D)J sequence was reconstructed using IMGT-gapped reference V,
418 D and J sequences.

419 **44m heavy chain SHM analysis using ARMADiLLO method**

420 To estimate the probability of amino acid SHM substitutions in the 44m heavy chain we used the
421 ARMADiLLO method as described previously[36].

422 **Antibody gene synthesis**

423 The antibody heavy chain genes of matured AIIMS-P01 lineage antibody was synthesized after
424 codon-optimization for mammalian expression from Genscript, Inc. USA, and cloned in respective
425 monoclonal antibody expression vector AbVec under AgeI and SalI sites[56].

426 **Antibody genes sequence analysis**

427 The sequencing of the antibody genes was done commercially from Eurofins, India. The sequences
428 were analyzed online through IMGT/V-QUEST (http://www.imgt.org/IMGT_vquest/vquest)[51].

429 **Expression of monoclonal antibodies**

430 All HIV-1 mAbs were expressed in Expi293F cells (Thermo Fisher) as described previously[22,57].
431 Briefly, 15μg each of heavy chain and light chain expressing IgG1 plasmids were co-transfected
432 using PEI-Max as transfection reagent. Following 4-6 days of incubation, cells were harvested by
433 centrifugation and filtered through 0.22 mm syringe filter (mdi). The supernatant was added to a
434 Protein A column affinity chromatography column (Pierce). The column was then washed with
435 1×PBS and mAbs were eluted with IgG Elution Buffer (Pierce), immediately neutralized with 1M
436 Tris pH 8.0 buffer and extensively dialyzed against 1×PBS at 4°C. The mAbs were then
437 concentrated using 10kDa Amicon Ultra-15 centrifugal filter units (EMD Millipore), filtered
438 through a 0.22 mm syringe filter (mdi) and stored at -80°C for further use.

439 **Expression and purification of HIV-1 trimeric proteins**

440 The BG505.SOSIP.664.T332N gp140 trimeric proteins with twin-strep-tag was expressed in HEK
441 293F cells and purified by methods described previously[58]. Briefly, SOSIP proteins were expressed
442 in transiently transfected HEK293F suspension cells (Invitrogen, cat no. R79009), maintained in
443 FreeStyle Expression Medium (Gibco). For transfection, HIV-1 Env and furin protease-encoding
444 plasmids were mixed in a 3:1 Env to furin ratio (w/w) were incubated with PEImax (Polysciences
445 Europe GmBH, Eppelheim, Germany) in a 3:1 (w/w) PEImax to DNA ratio and then added in the
446 supernatant of cells at a density of 1.2-1.5 million cells/mL. Six days post-transfection,
447 supernatants were harvested, centrifuged, and filtered using 0.22 μm pore size filters before
448 protein purification. HIV-1 env proteins were purified by immunoaffinity chromatography with
449 PGT145 antibody affinity column. Unpurified proteins contained in HEK293F filtered
450 supernatants were captured on PGT145-functionalized CNBr-activated sepharose 4B beads (GE
451 Healthcare) by overnight rolling incubation at 4 °C. Subsequently, the mixes of supernatant and
452 beads were passed over Econo-Column chromatography columns (Biorad). The column was then
453 washed with three column volumes of a 0.5 M NaCl and 20 mM Tris HCl pH 8.0 solution. After
454 elution with 3 M $MgCl_2$ pH 7.4, proteins were buffer-exchanged into TN75 (75 mM NaCl, 20 mM
455 Tris HCl pH 8.0) buffer by ultrafiltration with Vivaspin20 filters (Sartorius) of MWCO 100 kDa.
456 Protein concentrations were determined from the A280 values measured on a NanoDrop2000
457 device (Thermo Fisher Scientific) and the molecular weight and extinction coefficient values
458 calculated by the ProtParam Expasy webtool. Purity was assessed by blue native polyacrylamide
459 gel electrophoresis (BN-PAGE) and binding reactivity with HIV-1 bnAbs was assessed by ELISA.

460 **Binding analysis of mAbs by ELISA**

461 Briefly, 96-well ELISA plates (Costar) were coated with 5μg/ml recombinant HIV-1 gp120
462 monomeric proteins overnight at 4°C in 0.1 M $NaHCO_3$ (pH 9.6). Next day, plates were washed
463 thrice with 1×PBS (phosphate buffered saline) and blocked with 15% FBS RPMI and 2% BSA. After
464 1.5 hours of blocking at 37°C, plates were washed thrice with 1×PBS. Then, serial dilutions of
465 monoclonal antibodies (mAbs) were added and incubated for 1 hour at 37°C. Next, alkaline
466 phosphatase (AP) labelled anti-Fc secondary antibody (Southern Biotech) at 1:2,000 was added
467 and plates were incubated at 37°C for 1 hour. Plates were then washed thrice with 1×PBS and AP
468 substrate tablets (Sigma) dissolved in diethanolamine (DAE) was added and incubated for 30 min
469 at room temperature in the dark and readout was taken at 405nm. The BG505.SOSIP.664.T332N
470 gp140 trimeric ELISA was performed as described previously[58]. Briefly, purified twin-strep-tag
471 BG505.SOSIP.664.T332N gp140 protein (1 μg/mL) was diluted in PBS and captured on 96-well
472 Streptactin XT ELISA plates (IBA, Germany) followed by a 2 h incubation at room temperature.
473 Following two washes with 1x PBS to remove unbound trimers, serial dilutions of test antibodies
474 in PBS/2% skimmed milk were added and incubated for 2 h. After 3 washes with PBS, alkaline
475 phosphatase (AP) labelled anti-Fc secondary antibody (Southern Biotech) at 1:2,000 in PBS/2%
476 skimmed milk was added and incubated for 1 h, followed by 4 washes with PBS/0.05% Tween20.
477 Plates were then washed thrice with 1×PBS and AP substrate tablets (Sigma) dissolved in
478 diethanolamine (DAE) was added and incubated for 30 min at room temperature in the dark and
479 readout was taken at 405nm.

480 **HIV-1 pseudovirus generation**

481 The HIV-1 pseudoviruses were produced in HEK 293T cells as described earlier[20,22] by co-
482 transfecting the full HIV-1 gp160 envelope plasmid and a pSG3ΔEnv backbone plasmid. Briefly,
483 $1\times10^5$ cells in 2ml complete DMEM (10% fetal bovine serum (FBS) and 1% penicillin and
484 streptomycin antibiotics) were seeded per well of a 6 well cell culture plate (Costar) the day prior
485 to co-transfection for HIV-1 pseudovirus generation. For transfection, envelope (1.25μg) to delta
486 envelope plasmid (2.50μg) ratio was 1:2, this complex was made in Opti-MEM (Gibco) with a final
487 volume of 200μl for each well of the 6 well plate and incubated for 5 minutes at room temperature.
488 Next, 3μl of PEI-Max transfection reagent (Polysciences) (1mg/ml) was added to this mixture,
489 mixed well and further incubated for 15 min at room temperature. This mixture was then added
490 dropwise to HEK 293T cells supplemented with fresh complete DMEM growth media and

491 incubated at 37°C for 48 hours. Pseudoviruses were then harvested by filtering cell supernatants
492 with 0.45 mm sterile filter (mdi) and stored frozen at −80°C as aliquots.

493 **HIV-1 neutralization assays**

494 The HIV-1 neutralization assays of monoclonal antibodies (mAbs) were done as described
495 earlier[38,59]. Neutralization was measured as a reduction in luciferase gene expression after a single
496 round of infection of TZM-bl cells (NIH AIDS Reagent Program) with HIV-1 envelope
497 pseudoviruses. The $TCID_{50}$ of the HIV-1 pseudoviruses was calculated and 200 $TCID_{50}$ of the virus
498 was used in neutralization assays by incubating with 1:3 serially diluted mAbs starting at 10
499 μg/ml. After that, freshly trypsinized TZM-bl cells in growth medium (complete DMEM with 10%
500 FBS and 1% penicillin and streptomycin antibiotics) containing 50μg/ml DEAE Dextran and 1 mM
501 Indinavir (in case of primary isolates) at $10^5$ cells/well were added and plates were incubated at
502 37°C for 48 hours. Virus controls (cells with HIV-1 virus only) and cell controls (cells without virus
503 and antibody) were included. MuLV was used as a negative control. After the incubation of the
504 plates for 48 hours, luciferase activity was measured using the Bright-Glow Luciferase Assay
505 System (Promega). $IC_{50}$ for antibodies were calculated. Values were derived from a dose-response
506 curve fit with a non-linear function using the GraphPad Prism 9 software (San Diego, CA).

507 **Fab Fragment Preparation**

508 The Fab fragments were generated from 4 mg of 44m IgG antibody using a Fab Fragmentation Kit
509 (G Biosciences) according to manufacturer's protocol. Purity and size of Fab fragments were
510 assessed by SDS-PAGE.

511 **Octet BLI analysis**

512 Octet biolayer interferometry (BLI) was performed using an Octet Red96 instrument (ForteBio,
513 Inc.). A 5 μg/ml concentration of each mAb was captured on a protein A sensor and its binding
514 kinetics were tested with serial 2-fold diluted HIV-1 SOSIP trimer protein (100 nM to 6.25 nM).
515 The baseline was obtained by measurements taken for 60 s in BLI buffer (1x PBS and 0.05%
516 Tween-20), and then, the sensors were subjected to association phase immersion for 300 s in wells
517 containing serial dilutions of HIV-1 SOSIP protein. Then, the sensors were immersed in BLI buffer
518 for as long as 600 s to measure the dissociation phase. The mean Kon, Koff and apparent KD values
519 of the mAbs binding affinities for HIV-1 SOSIP envelope protein were calculated from all the

520 binding curves based on their global fit to a 1:1 Langmuir binding model using Octet software
521 version 12.0.

522 **Negative-stain EM**

523 To observe the binding pattern of 44m bnAb to BG505.SOSIP.664.T332N gp140 trimer and the
524 homogeneity of the complex, we first performed room temperature negative staining TEM. The
525 SEC purified complex of BG505.SOSIP.664.T332N gp140 trimer and 44m bnAb (1.2 mg/ml) was
526 diluted by 70 times for analysis. The 3.5 µl of sample mixture was put onto a glow discharged
527 carbon coated Cu grids for 30 secs (EM grid, 300 mesh, Electron Microscopy Sciences). After 1.5
528 min of incubation of the sample on the grid, the remained solvent was blotted and three drops of
529 1% uranyl acetate (Uranyl Acetate 98%, ACS Reagent, Polysciences, Inc.) was applied on the grid
530 for staining purpose. The excess stain was blotted after each addition and after air dried, the grid
531 was used for data collection with 120 kV Talos L120C electron microscope. Data acquisition was
532 performed using 4k x 4k Ceta camera at the magnification of 73kx and it is calibrated at
533 3.84Å/pixel. The collected images were processed in EMAN 2.1[60]. From these micrographs we
534 picked particles in both manual and automated mode, and its co-ordinates were extracted using
535 e2boxer.py in EMAN 2.1. Followed by, reference free 2D class averages were performed to analyze
536 different views of bnAb bound trimer complex. The cleaned particles after extraction were taken
537 for reference-free 2D class averages using simple_prime2D of SIMPLE 2.1 software[61] with a mask
538 diameter of 30 pixels at 3.84 Å/pix.

539 **Sample preparation for cryo-EM**

540 R1.2/1.3 300 mesh copper grids (Quantifoil) (Electron Microscopy Sciences) were glow
541 discharged at 20mA for 90 seconds before cryo-freezing. Three microliters of the SEC purified
542 complex of BG505.SOSIP.664.T332N gp140 trimer and 44m bnAb (1.2 mg/ml) was applied onto
543 the freshly glow discharged grid, and immediately blotted for 8.5 secs without any blot force just
544 after 10 secs of incubation to remove excess solvent in pre-equilibrated chamber of FEI Vitrobot
545 Mark IV plunger. The sample was plunged into the liquid ethane just after blotting.

546 **Cryo-EM data acquisition**

547 Cryo-EM data were collected using 200 kV TalosArctica transmission electron microscope
548 (Thermo Scientific™) equipped with Gatan K2 Summit Direct Electron Detector. Movies were
549 recorded automatically using Latitude-S (DigitalMicrograph - GMS 3.5) at nominal magnification

550 of 45,000x at the effective pixel size of 1.17 Å (*14*). Micrographs were acquired in counting mode
551 with a total dose of 60 $e^-$/Å2, with an exposure time of 8 sec distributed for 20 frames. A total of
552 3000 movies were acquired for the BG505.SOSIP.664.T332N gp140 trimer and 44m bnAbs protein
553 complexes respectively.

554 **CryoEM data analysis and model building**

555 Single-Particle Analysis (SPA) were performed for the acquired cryo-EM movies using the Relion
556 version 3.1[52]. At first, drift and gain corrections of the individual movies were performed with
557 MotionCorr2[62] and estimated Contrast transfer function (CTF) parameters using CTFFIND
558 4.1.13[63]. Subsequently, CTF estimated micrographs were subjected to analyze to eliminate bad
559 micrographs using cisTEM[64] and also, to remove poor resolution micrographs with a fit resolution
560 threshold of 7 Å. The particles from best micrographs were chosen for automated picking using
561 2D reference in Relion and extracted with the box sizes of 280 Å for the BG505.SOSIP.664.T332N
562 gp140 trimer and 44m bnAb complexes. After three rounds of rigorous 2D classification good
563 classes with high-resolution features of the complex were obtained as 1080743 particles. These
564 well-defined particles were selected for 3D classification with C3 symmetry. To achieve high
565 resolution, all particles belonging to the best classes of the complex was accounted for 3D auto-
566 refinement and followed by movie refinement. The sharpening for the 3D auto-refined maps was
567 performed with Relion 3.1[52] and PHENIX[48]. Overviews of cryo-EM data processing is shown in
568 **Table S3**. Global resolution of Fourier shell correlation (FSC) was estimated at the threshold of
569 0.143 and the estimation of local resolution were performed with ResMap, using two auto-refined
570 half maps.

571 Automated model building was iteratively done with Phenix Real Space Refinement. Only the Env
572 trimer (PDB ID: 5aco) was docked with cryo-EM maps using UCSF Chimera "Fit in map" tool. To
573 build the model for bnAb, the query sequences of the Fab was submitted to Swiss-Model and the
574 resultant model was also fitted in the EM maps. The structural statistics for cryo-EM map and
575 atomic model were analyzed using Phenix[48], EMringer[65], Molprobity[50], and UCSF chimera[66]. cryo-
576 EM map and atomic model were visualized using UCSF ChimeraX[49].

577 **QUANTIFICATION AND STATISTICAL ANALYSIS**

578 For all HIV-1 pseudoviruses neutralization assays, data were fitted asymmetric nonlinear
579 regression model to obtain the $IC_{50}$. All neutralization assays were repeated at least 2 times, and

data shown are from representative experiments. All statistical analysis was done with GraphPad Prism software version 9.

## ACKNOWLEDGMENTS

This antibody work was supported by Department of Biotechnology, India Indo-SA BT/PR2450/MED/29/1222/2017) grant awarded to K.L. The cryoEM work and consumables were supported by DBT BUILDER PROGRAM (BT/INF/22/SP22/844/2107), DST-FIST (SR/FST/LSII-039/2015) and SERB (SERB-EMR/2016/000608) grants awarded to S.D. S.K. is supported through DBT/Wellcome Trust India Alliance Early Career Fellowship grant IA/E/18/1/504307 (S.K.). We are very much thankful to NIH AIDS reagent program for HIV-1 research reagents, Neutralizing antibody consortium (NAC), IAVI, USA for HIV-1 neutralizing antibodies.

## AUTHOR CONTRIBUTIONS

Experimental work, data acquisition and analysis of data by S.Ku., S.D.S., A.C., P.B., S.S, S.Ka, R.L., S.D. Conceptualization and implementation by S.Ku., S.D.S., S.D. and K.L. Manuscript writing by S.Ku., S.D.S., A.C., S.D. and K.L. All authors reviewed the manuscript and approved the final version of the manuscript.

## DECLARATION OF INTERESTS

All the authors have read and approved the manuscript for publication. K.L., S.K., and R.L. have filed an Indian patent application for pediatric bnAb AIIMS-P01 described in the present study. Other authors declare no competing interests.

600 **REFERENCES**


601 1. Burton, D.R., and Hangartner, L. (2016). Broadly Neutralizing Antibodies to HIV and Their Role
602 in Vaccine Design. Annu. Rev. Immunol. *34*, 635–659. 10.1146/annurev-immunol-041015-
603 055515.

604 2. Kumar, S., Singh, S., and Luthra, K. (2023). An Overview of Human Anti-HIV-1 Neutralizing
605 Antibodies against Diverse Epitopes of HIV-1. ACS Omega *8*, 7252–7261.
606 10.1021/acsomega.2c07933.

607 3. Sok, D., and Burton, D.R. (2018). Recent progress in broadly neutralizing antibodies to HIV.
608 Nat. Immunol. *19*, 1179–1188. 10.1038/s41590-018-0235-7.

609 4. Euler, Z., and Schuitemaker, H. (2012). Cross-reactive broadly neutralizing antibodies: timing
610 is everything. Front. Immunol. *3*, 215. 10.3389/fimmu.2012.00215.

611 5. Simek, M.D., Rida, W., Priddy, F.H., Pung, P., Carrow, E., Laufer, D.S., Lehrman, J.K., Boaz, M.,
612 Tarragona-Fiol, T., Miiro, G., et al. (2009). Human immunodeficiency virus type 1 elite
613 neutralizers: individuals with broad and potent neutralizing activity identified by using a high-
614 throughput neutralization assay together with an analytical selection algorithm. J. Virol. *83*,
615 7337–7348. 10.1128/JVI.00110-09.

616 6. Andrabi, R., Bhiman, J.N., and Burton, D.R. (2018). Strategies for a multi-stage neutralizing
617 antibody-based HIV vaccine. Curr. Opin. Immunol. *53*, 143–151. 10.1016/j.coi.2018.04.025.

618 7. Burton, D.R. (2017). What Are the Most Powerful Immunogen Design Vaccine Strategies?
619 Reverse Vaccinology 2.0 Shows Great Promise. Cold Spring Harb. Perspect. Biol. *9*.
620 10.1101/cshperspect.a030262.

621 8. del Moral-Sánchez, I., Russell, R.A., Schermer, E.E., Cottrell, C.A., Allen, J.D., Torrents de la Peña,
622 A., LaBranche, C.C., Kumar, S., Crispin, M., Ward, A.B., et al. (2022). High thermostability
623 improves neutralizing antibody responses induced by native-like HIV-1 envelope trimers. Npj
624 Vaccines *7*, 1–12. 10.1038/s41541-022-00446-4.

625 9. Goo, L., Chohan, V., Nduati, R., and Overbaugh, J. (2014). Early development of broadly
626 neutralizing antibodies in HIV-1-infected infants. Nat. Med. *20*, 655–658. 10.1038/nm.3565.

627 10. Simonich, C.A., Williams, K.L., Verkerke, H.P., Williams, J.A., Nduati, R., Lee, K.K., and Overbaugh,
628 J. (2016). HIV-1 Neutralizing Antibodies with Limited Hypermutation from an Infant. Cell *166*,
629 77–87. 10.1016/j.cell.2016.05.055.

630 11. Khan, L., Makhdoomi, M.A., Kumar, S., Nair, A., Andrabi, R., Clark, B.E., Auyeung, K.,
631 Bhattacharya, J., Vajpayee, M., Wig, N., et al. (2015). Identification of CD4-Binding Site
632 Dependent Plasma Neutralizing Antibodies in an HIV-1 Infected Indian Individual. PloS One
633 *10*, e0125575. 10.1371/journal.pone.0125575.

634 12. Khan, L., Kumar, R., Thiruvengadam, R., Parray, H.A., Makhdoomi, M.A., Kumar, S., Aggarwal, H.,
635 Mohata, M., Hussain, A.W., Das, R., et al. (2017). Cross-neutralizing anti-HIV-1 human single
636 chain variable fragments(scFvs) against CD4 binding site and N332 glycan identified from a
637 recombinant phage library. Sci. Rep. *7*, 45163. 10.1038/srep45163.

13. Fouda, G.G., De Paris, K., Levy, O., Marchant, A., Gray, G., Permar, S., Marovich, M., and Singh, A. (2020). Immunological mechanisms of inducing HIV immunity in infants. Vaccine *38*, 411–415. 10.1016/j.vaccine.2019.11.011.

14. Ditse, Z., Muenchhoff, M., Adland, E., Jooste, P., Goulder, P., Moore, P.L., and Morris, L. (2018). HIV-1 SUBTYPE C INFECTED CHILDREN WITH EXCEPTIONAL NEUTRALIZATION BREADTH EXHIBIT POLYCLONAL RESPONSES TARGETING KNOWN EPITOPES. J. Virol. 10.1128/JVI.00878-18.

15. Makhdoomi, M.A., Khan, L., Kumar, S., Aggarwal, H., Singh, R., Lodha, R., Singla, M., Das, B.K., Kabra, S.K., and Luthra, K. (2017). Evolution of cross-neutralizing antibodies and mapping epitope specificity in plasma of chronic HIV-1-infected antiretroviral therapy-naïve children from India. J. Gen. Virol. *98*, 1879–1891. 10.1099/jgv.0.000824.

16. Mishra, N., Kumar, S., Singh, S., Bansal, T., Jain, N., Saluja, S., Kumar, R., Bhattacharyya, S., Palanichamy, J.K., Mir, R.A., et al. (2021). Cross-neutralization of SARS-CoV-2 by HIV-1 specific broadly neutralizing antibodies and polyclonal plasma. PLOS Pathog. *17*, e1009958. 10.1371/journal.ppat.1009958.

17. Mishra, N., Sharma, S., Dobhal, A., Kumar, S., Chawla, H., Singh, R., Makhdoomi, M.A., Das, B.K., Lodha, R., Kabra, S.K., et al. (2020). Broadly neutralizing plasma antibodies effective against autologous circulating viruses in infants with multivariant HIV-1 infection. Nat. Commun. *11*, 4409. 10.1038/s41467-020-18225-x.

18. Mishra, N., Sharma, S., Dobhal, A., Kumar, S., Chawla, H., Singh, R., Das, B.K., Kabra, S.K., Lodha, R., and Luthra, K. (2020). A Rare Mutation in an Infant-Derived HIV-1 Envelope Glycoprotein Alters Interprotomer Stability and Susceptibility to Broadly Neutralizing Antibodies Targeting the Trimer Apex. J. Virol. *94*, 10.1128/jvi.00814-20. 10.1128/jvi.00814-20.

19. Mishra, N., Sharma, S., Dobhal, A., Kumar, S., Chawla, H., Singh, S., Singh, R., Das, B.K., Lodha, R., Kabra, S.K., et al. (2020). Plasma neutralizing antibodies in an infant with interclade HIV-1 superinfection preferentially neutralize superinfecting HIV-1 strains. 2020.12.10.420703. 10.1101/2020.12.10.420703.

20. Mishra, N., Makhdoomi, M.A., Sharma, S., Kumar, S., Dobhal, A., Kumar, D., Chawla, H., Singh, R., Kanga, U., Das, B.K., et al. (2019). Viral characteristics associated with maintenance of elite neutralizing activity in chronically HIV-1 clade C infected monozygotic pediatric twins. J. Virol., JVI.00654-19. 10.1128/JVI.00654-19.

21. Muenchhoff, M., Prendergast, A.J., and Goulder, P.J.R. (2014). Immunity to HIV in Early Life. Front. Immunol. *5*, 391. 10.3389/fimmu.2014.00391.

22. Kumar, S., Panda, H., Makhdoomi, M.A., Mishra, N., Safdari, H.A., Chawla, H., Aggarwal, H., Reddy, E.S., Lodha, R., Kumar Kabra, S., et al. (2019). An HIV-1 Broadly Neutralizing Antibody from a Clade C-Infected Pediatric Elite Neutralizer Potently Neutralizes the Contemporaneous and Autologous Evolving Viruses. J. Virol. *93*. 10.1128/JVI.01495-18.

23. Scheid, J.F., Mouquet, H., Ueberheide, B., Diskin, R., Klein, F., Oliveira, T.Y.K., Pietzsch, J., Fenyo, D., Abadir, A., Velinzon, K., et al. (2011). Sequence and structural convergence of broad and potent HIV antibodies that mimic CD4 binding. Science *333*, 1633–1637. 10.1126/science.1207227.

679 24. Freund, N.T., Wang, H., Scharf, L., Nogueira, L., Horwitz, J.A., Bar-On, Y., Golijanin, J., Sievers,
680 S.A., Sok, D., Cai, H., et al. (2017). Coexistence of potent HIV-1 broadly neutralizing antibodies
681 and antibody-sensitive viruses in a viremic controller. Sci. Transl. Med. *9*.
682 10.1126/scitranslmed.aal2144.

683 25. Walker, L.M., Phogat, S.K., Chan-Hui, P.-Y., Wagner, D., Phung, P., Goss, J.L., Wrin, T., Simek, M.D.,
684 Fling, S., Mitcham, J.L., et al. (2009). Broad and potent neutralizing antibodies from an African
685 donor reveal a new HIV-1 vaccine target. Science *326*, 285–289. 10.1126/science.1178746.

686 26. Walker, L.M., Huber, M., Doores, K.J., Falkowska, E., Pejchal, R., Julien, J.-P., Wang, S.-K., Ramos,
687 A., Chan-Hui, P.-Y., Moyle, M., et al. (2011). Broad neutralization coverage of HIV by multiple
688 highly potent antibodies. Nature *477*, 466–470. 10.1038/nature10373.

689 27. Huang, J., Ofek, G., Laub, L., Louder, M.K., Doria-Rose, N.A., Longo, N.S., Imamichi, H., Bailer, R.T.,
690 Chakrabarti, B., Sharma, S.K., et al. (2012). Broad and potent neutralization of HIV-1 by a gp41-
691 specific human antibody. Nature *491*, 406–412. 10.1038/nature11544.

692 28. Huang, J., Kang, B.H., Ishida, E., Zhou, T., Griesman, T., Sheng, Z., Wu, F., Doria-Rose, N.A., Zhang,
693 B., McKee, K., et al. (2016). Identification of a CD4-Binding-Site Antibody to HIV that Evolved
694 Near-Pan Neutralization Breadth. Immunity *45*, 1108–1121. 10.1016/j.immuni.2016.10.027.

695 29. Bonsignori, M., Kreider, E.F., Fera, D., Meyerhoff, R.R., Bradley, T., Wiehe, K., Alam, S.M.,
696 Aussedat, B., Walkowicz, W.E., Hwang, K.-K., et al. (2017). Staged induction of HIV-1 glycan-
697 dependent broadly neutralizing antibodies. Sci. Transl. Med. *9*. 10.1126/scitranslmed.aai7514.

698 30. Falkowska, E., Le, K.M., Ramos, A., Doores, K.J., Lee, J.H., Blattner, C., Ramirez, A., Derking, R.,
699 van Gils, M.J., Liang, C.-H., et al. (2014). Broadly neutralizing HIV antibodies define a glycan-
700 dependent epitope on the prefusion conformation of gp41 on cleaved envelope trimers.
701 Immunity *40*, 657–668. 10.1016/j.immuni.2014.04.009.

702 31. Schoofs, T., Barnes, C.O., Suh-Toma, N., Golijanin, J., Schommers, P., Gruell, H., West, A.P., Bach,
703 F., Lee, Y.E., Nogueira, L., et al. (2019). Broad and Potent Neutralizing Antibodies Recognize the
704 Silent Face of the HIV Envelope. Immunity *50*, 1513-1529.e9. 10.1016/j.immuni.2019.04.014.

705 32. Doria-Rose, N.A., Bhiman, J.N., Roark, R.S., Schramm, C.A., Gorman, J., Chuang, G.-Y., Pancera, M.,
706 Cale, E.M., Ernandes, M.J., Louder, M.K., et al. (2016). New Member of the V1V2-Directed
707 CAP256-VRC26 Lineage That Shows Increased Breadth and Exceptional Potency. J. Virol. *90*,
708 76–91. 10.1128/JVI.01791-15.

709 33. Aggarwal, H., Khan, L., Chaudhary, O., Kumar, S., Makhdoomi, M.A., Singh, R., Sharma, K., Mishra,
710 N., Lodha, R., Srinivas, M., et al. (2017). Alterations in B Cell Compartment Correlate with Poor
711 Neutralization Response and Disease Progression in HIV-1 Infected Children. Front. Immunol.
712 *8*, 1697. 10.3389/fimmu.2017.01697.

713 34. Kumar, S., Kumar, R., Khan, L., Makhdoomi, M.A., Thiruvengadam, R., Mohata, M., Agarwal, M.,
714 Lodha, R., Kabra, S.K., Sinha, S., et al. (2017). CD4-Binding Site Directed Cross-Neutralizing scFv
715 Monoclonals from HIV-1 Subtype C Infected Indian Children. Front. Immunol. *8*, 1568.
716 10.3389/fimmu.2017.01568.

717 35. Kumar, S., Bajpai, P., Joyce, C., Kabra, S.K., Lodha, R., Burton, D., Briney, B., and Luthra, P.K.
718 (2023). B cell repertoire sequencing of HIV–1 pediatric elite–neutralizers identifies multiple
719 broadly neutralizing antibody clonotypes. 2023.07.07.548149. 10.1101/2023.07.07.548149.

720 36. Martin Beem, J.S., Venkatayogi, S., Haynes, B.F., and Wiehe, K. (2023). ARMADiLLO: a web
721 server for analyzing antibody mutation probabilities. Nucleic Acids Res. *51*, W51–W56.
722 10.1093/nar/gkad398.

723 37. Wiehe, K., Bradley, T., Meyerhoff, R.R., Hart, C., Williams, W.B., Easterhoff, D., Faison, W.J.,
724 Kepler, T.B., Saunders, K.O., Alam, S.M., et al. (2018). Functional Relevance of Improbable
725 Antibody Mutations for HIV Broadly Neutralizing Antibody Development. Cell Host Microbe
726 *23*, 759-765.e6. 10.1016/j.chom.2018.04.018.

727 38. Montefiori, D.C. (2009). Measuring HIV neutralization in a luciferase reporter gene assay.
728 Methods Mol. Biol. Clifton NJ *485*, 395–405. 10.1007/978-1-59745-170-3_26.

729 39. Mouquet, H., Scharf, L., Euler, Z., Liu, Y., Eden, C., Scheid, J.F., Halper-Stromberg, A.,
730 Gnanapragasam, P.N.P., Spencer, D.I.R., Seaman, M.S., et al. (2012). Complex-type N-glycan
731 recognition by potent broadly neutralizing HIV antibodies. Proc. Natl. Acad. Sci. U. S. A. *109*,
732 E3268-3277. 10.1073/pnas.1217207109.

733 40. Setliff, I., McDonnell, W.J., Raju, N., Bombardi, R.G., Murji, A.A., Scheepers, C., Ziki, R., Mynhardt,
734 C., Shepherd, B.E., Mamchak, A.A., et al. (2018). Multi-Donor Longitudinal Antibody Repertoire
735 Sequencing Reveals the Existence of Public Antibody Clonotypes in HIV-1 Infection. Cell Host
736 Microbe *23*, 845-854.e6. 10.1016/j.chom.2018.05.001.

737 41. Willis, J.R., Berndsen, Z.T., Ma, K.M., Steichen, J.M., Schiffner, T., Landais, E., Liguori, A.,
738 Kalyuzhniy, O., Allen, J.D., Baboo, S., et al. (2022). Human immunoglobulin repertoire analysis
739 guides design of vaccine priming immunogens targeting HIV V2-apex broadly neutralizing
740 antibody precursors. Immunity *0*. 10.1016/j.immuni.2022.09.001.

741 42. Sok, D., Laserson, U., Laserson, J., Liu, Y., Vigneault, F., Julien, J.-P., Briney, B., Ramos, A., Saye,
742 K.F., Le, K., et al. (2013). The effects of somatic hypermutation on neutralization and binding
743 in the PGT121 family of broadly neutralizing HIV antibodies. PLoS Pathog. *9*, e1003754.
744 10.1371/journal.ppat.1003754.

745 43. Bonsignori, M., Zhou, T., Sheng, Z., Chen, L., Gao, F., Joyce, M.G., Ozorowski, G., Chuang, G.-Y.,
746 Schramm, C.A., Wiehe, K., et al. (2016). Maturation Pathway from Germline to Broad HIV-1
747 Neutralizer of a CD4-Mimic Antibody. Cell *165*, 449–463. 10.1016/j.cell.2016.02.022.

748 44. Sok, D., van Gils, M.J., Pauthner, M., Julien, J.-P., Saye-Francisco, K.L., Hsueh, J., Briney, B., Lee,
749 J.H., Le, K.M., Lee, P.S., et al. (2014). Recombinant HIV envelope trimer selects for quaternary-
750 dependent antibodies targeting the trimer apex. Proc. Natl. Acad. Sci. U. S. A. *111*, 17624–
751 17629. 10.1073/pnas.1415789111.

752 45. Julien, J.-P., Sok, D., Khayat, R., Lee, J.H., Doores, K.J., Walker, L.M., Ramos, A., Diwanji, D.C.,
753 Pejchal, R., Cupo, A., et al. (2013). Broadly neutralizing antibody PGT121 allosterically
754 modulates CD4 binding via recognition of the HIV-1 gp120 V3 base and multiple surrounding
755 glycans. PLoS Pathog. *9*, e1003342. 10.1371/journal.ppat.1003342.

756 46. Dingens, A.S., Arenz, D., Weight, H., Overbaugh, J., and Bloom, J.D. (2019). An Antigenic Atlas of
757 HIV-1 Escape from Broadly Neutralizing Antibodies Distinguishes Functional and Structural
758 Epitopes. Immunity *50*, 520-532.e3. 10.1016/j.immuni.2018.12.017.

759 47. Emsley, P., Lohkamp, B., Scott, W.G., and Cowtan, K. (2010). Features and development of Coot.
760 Acta Crystallogr. D Biol. Crystallogr. *66*, 486–501. 10.1107/S0907444910007493.

761 48. Adams, P.D., Afonine, P.V., Bunkóczi, G., Chen, V.B., Davis, I.W., Echols, N., Headd, J.J., Hung, L.-
762 W., Kapral, G.J., Grosse-Kunstleve, R.W., et al. (2010). PHENIX: a comprehensive Python-based
763 system for macromolecular structure solution. Acta Crystallogr. D Biol. Crystallogr. *66*, 213–
764 221. 10.1107/S0907444909052925.

765 49. Goddard, T.D., Huang, C.C., Meng, E.C., Pettersen, E.F., Couch, G.S., Morris, J.H., and Ferrin, T.E.
766 (2018). UCSF ChimeraX: Meeting modern challenges in visualization and analysis. Protein Sci.
767 Publ. Protein Soc. *27*, 14–25. 10.1002/pro.3235.

768 50. Williams, C.J., Headd, J.J., Moriarty, N.W., Prisant, M.G., Videau, L.L., Deis, L.N., Verma, V., Keedy,
769 D.A., Hintze, B.J., Chen, V.B., et al. (2018). MolProbity: More and better reference data for
770 improved all-atom structure validation. Protein Sci. Publ. Protein Soc. *27*, 293–315.
771 10.1002/pro.3330.

772 51. Lefranc, M.-P., Giudicelli, V., Ginestoux, C., Jabado-Michaloud, J., Folch, G., Bellahcene, F., Wu, Y.,
773 Gemrot, E., Brochet, X., Lane, J., et al. (2009). IMGT, the international ImMunoGeneTics
774 information system. Nucleic Acids Res. *37*, D1006-1012. 10.1093/nar/gkn838.

775 52. Scheres, S.H.W. (2012). RELION: Implementation of a Bayesian approach to cryo-EM structure
776 determination. J. Struct. Biol. *180*, 519–530. 10.1016/j.jsb.2012.09.006.

777 53. Briney, B., Inderbitzin, A., Joyce, C., and Burton, D.R. (2019). Commonality despite exceptional
778 diversity in the baseline human antibody repertoire. Nature *566*, 393–397. 10.1038/s41586-
779 019-0879-y.

780 54. Gupta, N.T., Vander Heiden, J.A., Uduman, M., Gadala-Maria, D., Yaari, G., and Kleinstein, S.H.
781 (2015). Change-O: a toolkit for analyzing large-scale B cell immunoglobulin repertoire
782 sequencing data. Bioinforma. Oxf. Engl. *31*, 3356–3358. 10.1093/bioinformatics/btv359.

783 55. Vander Heiden, J.A., Yaari, G., Uduman, M., Stern, J.N.H., O'Connor, K.C., Hafler, D.A., Vigneault,
784 F., and Kleinstein, S.H. (2014). pRESTO: a toolkit for processing high-throughput sequencing
785 raw reads of lymphocyte receptor repertoires. Bioinformatics *30*, 1930–1932.
786 10.1093/bioinformatics/btu138.

787 56. Smith, K., Garman, L., Wrammert, J., Zheng, N.-Y., Capra, J.D., Ahmed, R., and Wilson, P.C. (2009).
788 Rapid generation of fully human monoclonal antibodies specific to a vaccinating antigen. Nat.
789 Protoc. *4*, 372–384. 10.1038/nprot.2009.3.

790 57. Kumar, S., Patel, A., Lai, L., Chakravarthy, C., Valanparambil, R., Reddy, E.S., Gottimukkala, K.,
791 Davis-Gardner, M.E., Edara, V.V., Linderman, S., et al. (2022). Structural insights for
792 neutralization of Omicron variants BA.1, BA.2, BA.4, and BA.5 by a broadly neutralizing SARS-
793 CoV-2 antibody. Sci. Adv. *8*, eadd2032. 10.1126/sciadv.add2032.

794 58. Sanders, R.W., Derking, R., Cupo, A., Julien, J.-P., Yasmeen, A., de Val, N., Kim, H.J., Blattner, C., de
795 la Peña, A.T., Korzun, J., et al. (2013). A next-generation cleaved, soluble HIV-1 Env trimer,
796 BG505 SOSIP.664 gp140, expresses multiple epitopes for broadly neutralizing but not non-
797 neutralizing antibodies. PLoS Pathog. *9*, e1003618. 10.1371/journal.ppat.1003618.

798 59. Kumar, S., Batra, H., Singh, S., Chawla, H., Singh, R., Katpara, S., Hussain, A.W., Das, B.K., Lodha,
799 R., Kabra, S.K., et al. (2020). Effect of combination antiretroviral therapy on human
800 immunodeficiency virus 1 specific antibody responses in subtype-C infected children. J. Gen.
801 Virol. *101*, 1289–1299. 10.1099/jgv.0.001480.

802 60. Bell, J.M., Chen, M., Baldwin, P.R., and Ludtke, S.J. (2016). High resolution single particle
803 refinement in EMAN2.1. Methods San Diego Calif *100*, 25–34. 10.1016/j.ymeth.2016.02.018.

804 61. Reboul, C.F., Eager, M., Elmlund, D., and Elmlund, H. (2018). Single-particle cryo-EM-Improved
805 ab initio 3D reconstruction with SIMPLE/PRIME. Protein Sci. Publ. Protein Soc. *27*, 51–61.
806 10.1002/pro.3266.

807 62. Zheng, S.Q., Palovcak, E., Armache, J.-P., Verba, K.A., Cheng, Y., and Agard, D.A. (2017).
808 MotionCor2: anisotropic correction of beam-induced motion for improved cryo-electron
809 microscopy. Nat. Methods *14*, 331–332. 10.1038/nmeth.4193.

810 63. Rohou, A., and Grigorieff, N. (2015). CTFFIND4: Fast and accurate defocus estimation from
811 electron micrographs. J. Struct. Biol. *192*, 216–221. 10.1016/j.jsb.2015.08.008.

812 64. Grant, T., Rohou, A., and Grigorieff, N. (2018). cisTEM, user-friendly software for single-particle
813 image processing. eLife *7*, e35383. 10.7554/eLife.35383.

814 65. Barad, B.A., Echols, N., Wang, R.Y.-R., Cheng, Y., DiMaio, F., Adams, P.D., and Fraser, J.S. (2015).
815 EMRinger: side chain–directed model and map validation for 3D cryo-electron microscopy.
816 Nat. Methods *12*, 943–946. 10.1038/nmeth.3541.

817 66. Pettersen, E.F., Goddard, T.D., Huang, C.C., Couch, G.S., Greenblatt, D.M., Meng, E.C., and Ferrin,
818 T.E. (2004). UCSF Chimera--a visualization system for exploratory research and analysis. J.
819 Comput. Chem. *25*, 1605–1612. 10.1002/jcc.20084.

820

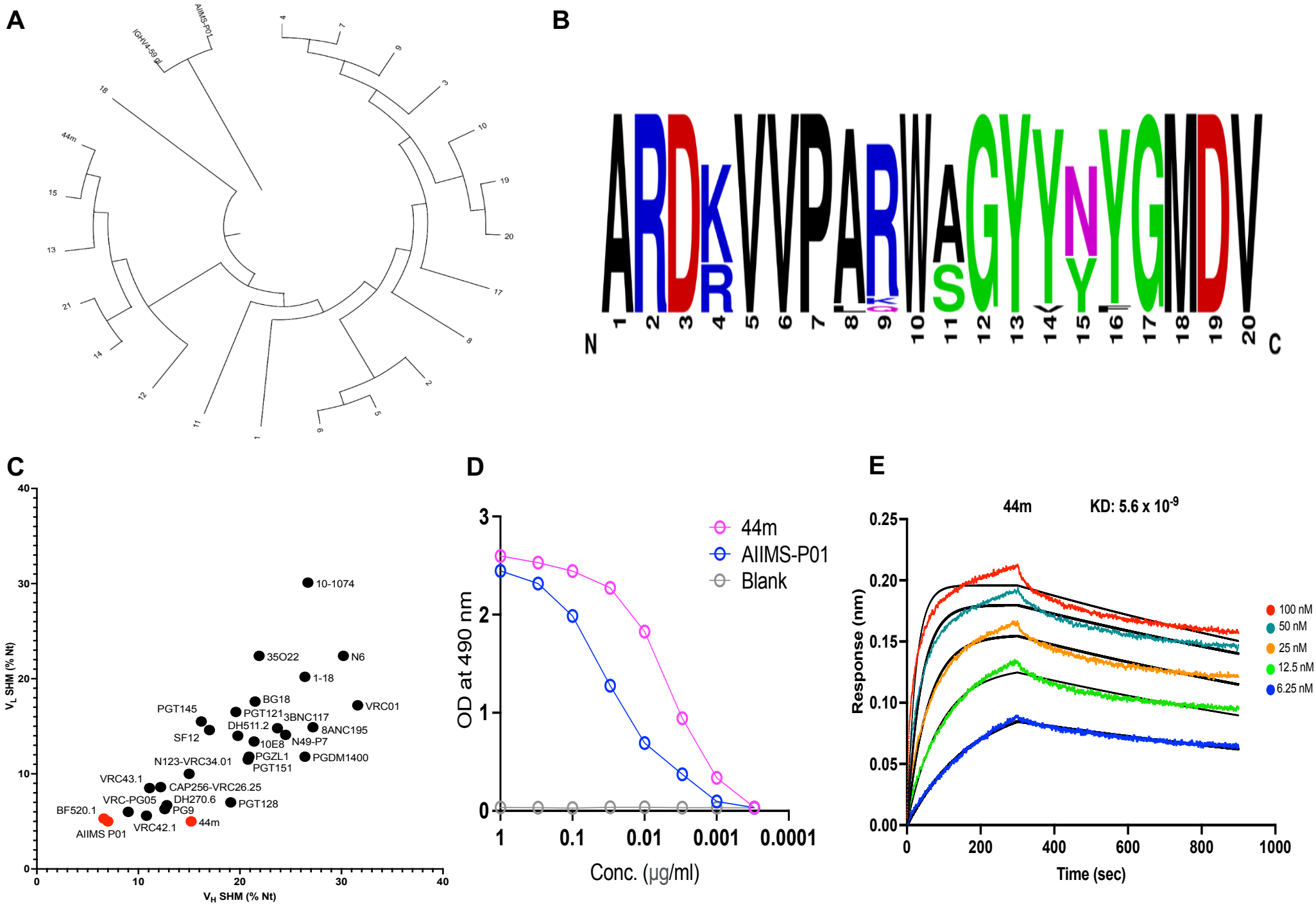
A
AIIMS-P01
IGHV4-59 gl
44m
B
N
C
C
10-1074
35O22
N6
1-18
BG18
VRC01
PGT145
PGT121
3BNC117
DH511.2
8ANC195
SF12
10E8
N49-P7
N123-VRC34.01
PGZL1
PGDM1400
PGT151
VRC43.1
CAP256-VRC26.25
VRC-PG05
DH270.6
PGT128
BF520.1
PG9
44m
AIIMS P01
VRC42.1
$V_L$ SHM (% Nt)
$V_H$ SHM (% Nt)
D
44m
AIIMS-P01
Blank
OD at 490 nm
Conc. (µg/ml)
E
44m
KD: 5.6 x $10^{-9}$
100 nM
50 nM
25 nM
12.5 nM
6.25 nM
Response (nm)
Time (sec)

**A**

| S.No. | Virus ID | Tier | Clade | AIIMS-P01 | 44m |
|---|---|---|---|---|---|
| 1 | QB726.70.M env C4 | 1B | A | >10 | 0.15 |
| 2 | Q769.ENV H5 | 1B | A | >10 | 0.6 |
| 3 | 700010058.A4.4375 | 1B | B | 2.5 | 0.35 |
| 4 | SF162 | 1A | B | 0.023 | 0.022 |
| 5 | CAAN | 2 | B | 1.55 | 0.1 |
| 6 | WITO | 2 | B | >10 | >10 |
| 7 | TRJO | 3 | B | >10 | >10 |
| 8 | RHPA | 2 | B | 4.1 | 0.5 |
| 9 | TR011 | 2 | B | 3 | 0.2 |
| 10 | AC10 | 2 | B | >10 | 0.65 |
| 11 | QHO692 | 2 | B | >10 | 2.7 |
| 12 | SC422661.8 | 2 | B | 4.65 | 0.95 |
| 13 | 1012.TC21.3257 | 1B | B | >10 | 0.6 |
| 14 | 1059_09.A4.1460 | 2 | B | >10 | 9.55 |
| 15 | PRB931_06.TC3.4930 | 1B | B | 0.4 | 0.05 |
| 16 | 6244_13.B5.4576 | 2 | B | 9.4 | 0.9 |
| 17 | 6240_08.TA5.4622 | 2 | B | 2.1 | 0.2 |
| 18 | 63358.p3.4013 | 2 | B | >10 | 0.3 |
| 19 | THRO | 2 | B | >10 | >10 |
| 20 | PRB958_06.TB1.4305 | 2 | B | 3.1 | 0.35 |
| 21 | SC45.4B5.2631 | 2 | B | >10 | 0.25 |
| 22 | WEAUd15.410.5017 | 2 | B | 3.05 | 0.2 |
| 23 | REJO | 2 | B | >10 | >10 |
| 24 | ZM197 | 1B | C (African) | >10 | >10 |
| 25 | ZM214 | 2 | C (African) | >10 | >10 |
| 26 | ZM233 | 2 | C (African) | 1 | 0.07 |
| 27 | ZM53 | 2 | C (African) | >10 | >10 |
| 28 | ZM109 | 1B | C (African) | >10 | >10 |
| 29 | ZM249 | 2 | C (African) | >10 | >10 |
| 30 | QC406 envF3 | 2 | C (African) | 0.55 | 0.01 |
| 31 | CAP45 | 2 | C (African) | >10 | >10 |
| 32 | CAP210 | 2 | C (African) | >10 | >10 |
| 33 | Du156 | 2 | C (African) | 0.15 | 0.25 |
| 34 | Du172 | 2 | C (African) | 1.93 | 1.18 |
| 35 | Du422.1 | 2 | C (African) | 1.21 | 0.41 |
| 36 | MJ412 | 2 | C (African) | 0.031 | 0.054 |
| 37 | 16055 | 2 | C (Indian) | >10 | >10 |
| 38 | 25710 | 1 | C (Indian) | 1.2 | 0.7 |
| 39 | 25711 | 1B | C (Indian) | 0.033 | 0.086 |
| 40 | 25925 | 1B | C (Indian) | 0.107 | 0.04 |
| 41 | 26191 | 2 | C (Indian) | >10 | 4.75 |
| 42 | 836 | 1A | C (Indian) | >10 | 0.01 |
| 43 | 16936 | 2 | C (Indian) | 1.4 | 5.55 |
| 44 | 70606F | 2 | C (Indian) | >10 | 3 |
| 45 | 70607Z | 2 | C (Indian) | >10 | 3.8 |
| 46 | 70607B | 2 | C (Indian) | >10 | 0.6 |
| 47 | 70606B | 2 | C (Indian) | 9.95 | 0.9 |
| 48 | 70604B | 2 | C (Indian) | 9.93 | 0.75 |
| 49 | 70607C | 2 | C (Indian) | >10 | 1.2 |
| 50 | 70406 | 2 | C (Indian) | >10 | 3.4 |
| 51 | 70408 | 2 | C (Indian) | >10 | 3.25 |
| 52 | 70402 | 2 | C (Indian) | >10 | 1.65 |
| 53 | 709316B | 3 | C (Indian) | >10 | 3.3 |
| 54 | UZ12A | 2 | C (Indian) | >10 | 1.55 |
| 55 | 329.14.B1 | 2 | C (Indian) | 0.035 | 0.03 |
| 56 | 330.16.E6 | 2 | C (Indian) | 0.163 | 0.078 |
| 57 | MK184 | 2 | CD | 0.79 | 0.04 |
| 58 | BK184 | 2 | CD | 0.05 | 0.02 |
| | | GMT | | 0.74 | 0.52 | 0.36 |
| | | Breadth | | 46.50% | 41.30% | 79.30% |

| IC50 Color code (ug/ml) |
|---|
| < 1 |
| 14 |
| 5-10 |
| >10 |

**B**

| GLOBAL PANEL | | | | | |
|---|---|---|---|---|---|
| S.No. | Virus ID | Tier | Clade | AIIMS-P01 | 44m |
| 1 | CNE55 | 3 | AE | >10 | >10 |
| 2 | TRO11 | 2 | B | 1.5 | 1.15 |
| 3 | CNE8 | 2 | AE | >10 | >10 |
| 4 | CH119 | 2 | BC | 0.75 | 0.45 |
| 5 | 25710 | 1B | C | 1.2 | 0.7 |
| 6 | X2278 | 2 | B | 5.7 | 1.41 |
| 7 | 246F3 | 3 | A/C | >10 | >10 |
| 8 | X1632 | 2 | G | >10 | >10 |
| 9 | CE1176 | 2 | C | 0.8 | 0.26 |
| 10 | 398F1 | 2 | A | 0.25 | 0.16 |
| 11 | CEO217 | 3 | C | >10 | >10 |
| 12 | BJOX 2000 | 2 | BC | 0.25 | 0.15 |
| | GMT | | | 0.87 | 0.44 |
| | Breadth | | | 58% | 58% |

**C**

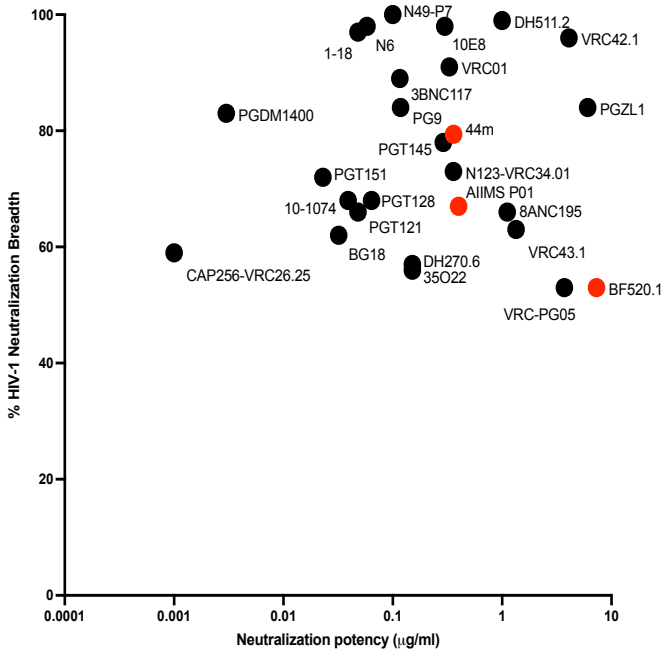

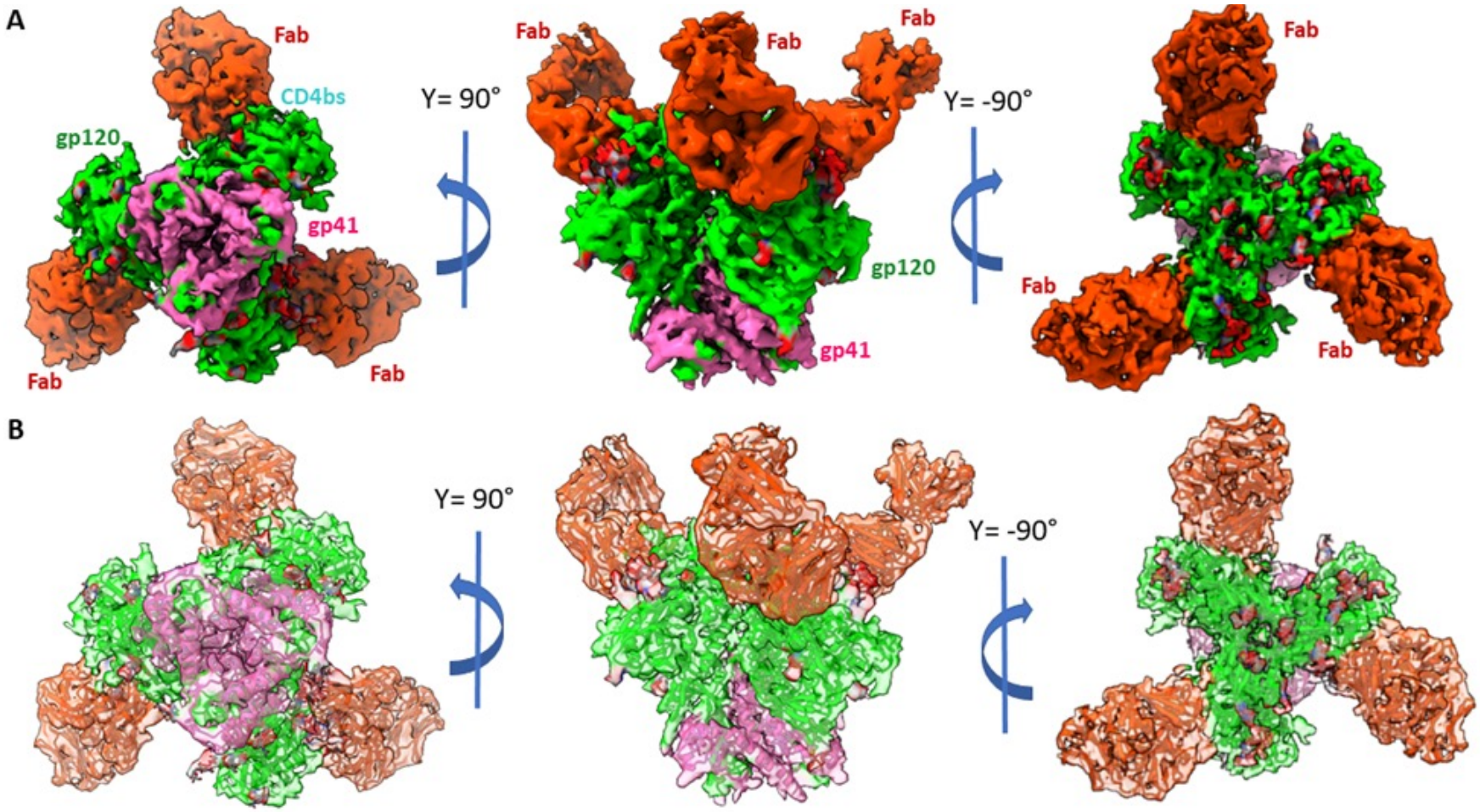
A
Fab
CD4bs
gp120
gp41
Fab
Fab
Y= 90°
Fab
Fab
Fab
gp120
gp41
Y= -90°
Fab
Fab
Fab
B
Y= 90°
Y= -90°

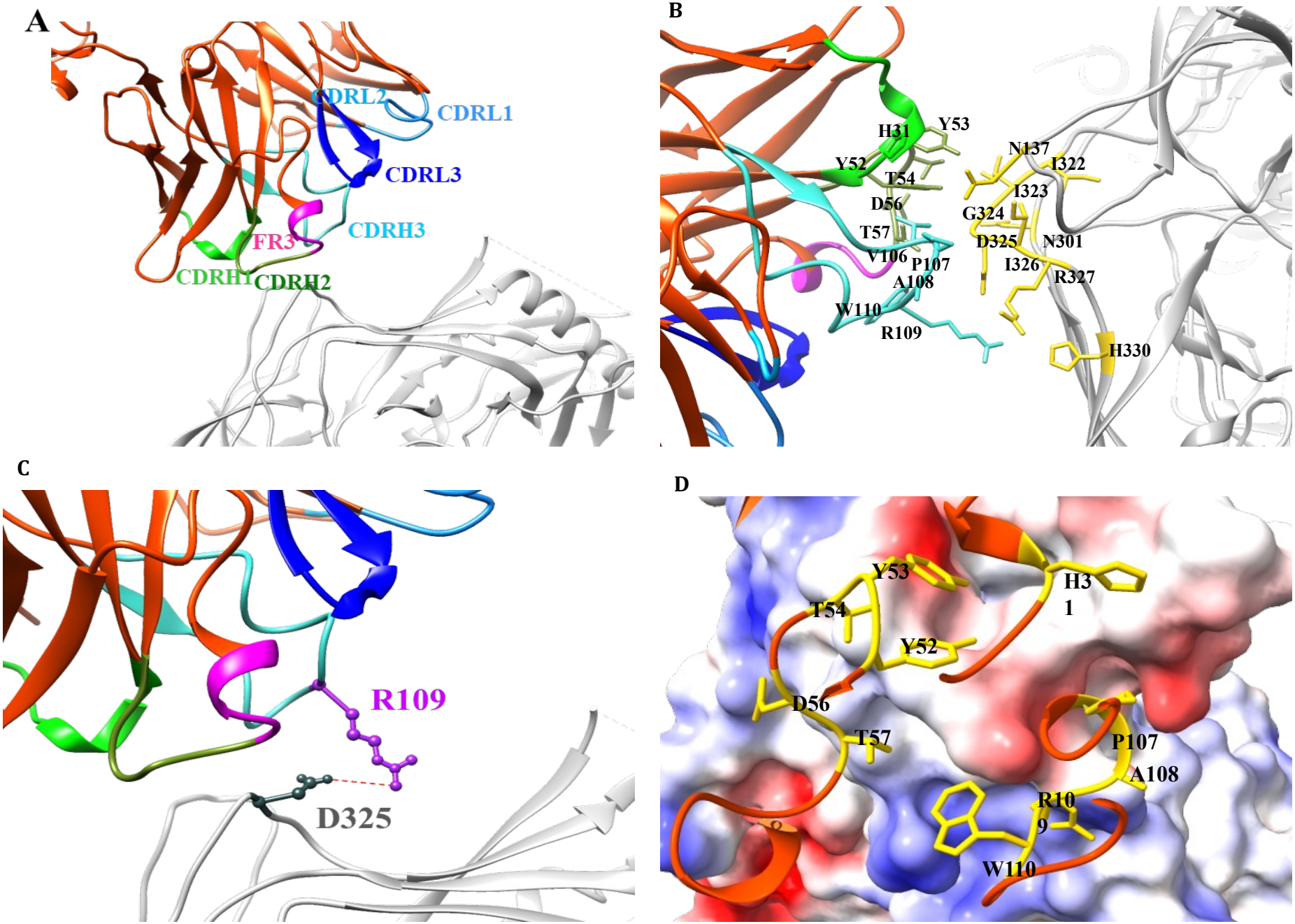
A
CDRL2
CDRL1
CDRL3
CDRH3
FR3
CDRH1
CDRH2
B
H31
Y53
Y52
T54
D56
T57
V106
P107
A108
W110
R109
N137
I322
I323
G324
D325
N301
I326
R327
H330
C
R109
D325
D
Y53
H3
1
T54
Y52
D56
T57
P107
A108
R10
9
W110

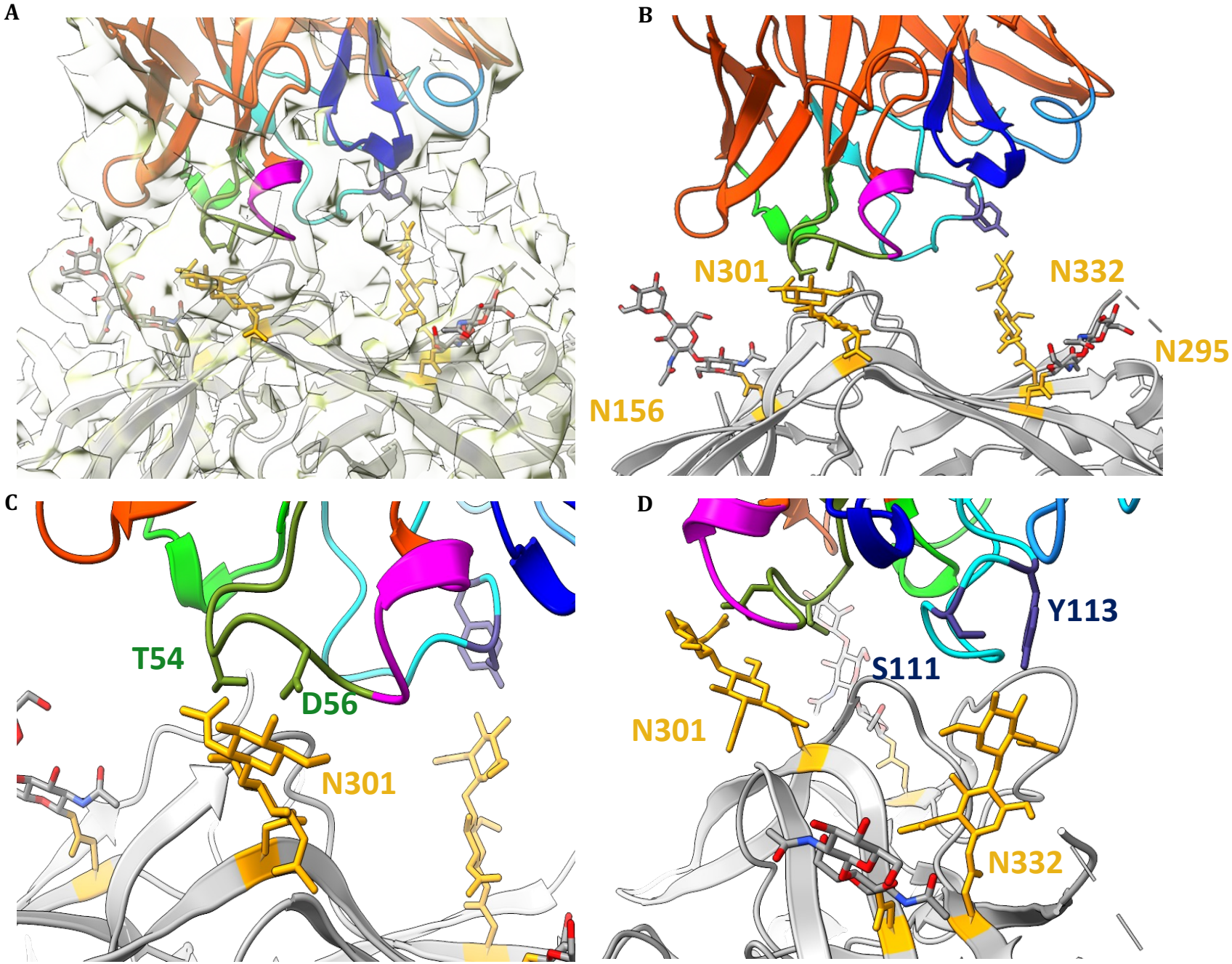
A
B
N301
N332
N295
N156
C
T54
D56
N301
D
Y113
S111
N301
N332